Journal of Thermal Analysis and Calorimetry (2023) 148:8323–8344
https://doi.org/10.1007/s10973-022-11765-y

Investigation of a hybridized combined cycle engine with SOFC system for marine applications

Shaimaa Seyam[1] · Ibrahim Dincer[1] · Martin Agelin-Chaab[1]

Received: 1 September 2022 / Accepted: 26 October 2022 / Published online: 24 November 2022

Abstract

Marine transportation facilitates the transportation of fuels and goods over long distances cost-effectively, but their environmental impact has increased due to the utilization of fossil fuels. This paper presents a new marine engine design comprising a steam Rankine cycle, gas Brayton cycle, and solid oxide fuel cell to replace a two-stroke internal combustion engine. Hydrogen, methane, dimethyl ether, ethanol, and methanol are selected as eco-friendly fuels. This hybrid combined engine is attached to a multi-effect desalination unit to take the advantage of waste energy from the exhaust gases. The engine is thermodynamically analyzed using the Aspen Plus software to assess its performance energetically and exergetically. It is found that the engine's total power is increased by 40% to an average of 15,546 kW with average thermal and exergetic efficiencies of 61% and 43%, respectively. The maximum power reaches 16,780 kW with maximum carbon emission reductions of 53% and a minimum specific fuel consumption of 337 g kWh^{-1} which is a reduction of 17%. In addition, the waste energy is used to deliver 20.3 kg s^{-1} freshwater by desalinating seawater. The proposed engine system has better performance and less environmental impact, which makes it a better choice than traditional engines.

Keywords Hydrogen · Steam Rankine cycle · Gas Brayton cycle · Solid oxide fuel cell · Energy · Exergy · Multi-effect desalination

List of symbols

A	Area (cm^2)
D	Diffusivity ($m^2\ s^{-1}$)
E	Nernst voltage (V)
$\dot{E}$	Energy rate (kW)
ex	Specific physical/chemical exergy flow
$\dot{E}x$	Exergy flow (kw)
F	Faraday constant ($C\ mol^{-1}$)
$\overline{g}$	Gibbs free energy ($kJ\ mol^{-1}$)
h	Specific enthalpy ($kJ\ kg^{-1}$)
i	Current density ($A\ cm^{-2}$)
I	Thermoelectric current (A)
N	Number of cells/stacks
$\dot{m}$	Mass flow rate ($kg\ s^{-1}$)
P	Pressure (kPa)
$\dot{Q}$	Heat rate (kW)
$\overline{R}$	Molar gas constant ($J\ mol^{-1}\ K^{-1}$)
s	Specific entropy ($kJ\ kg^{-1}\ K^{-1}$)
T	Temperature (K)
V	Voltage (V)
$\dot{W}$	Power (kW)

Subscripts

an	Anode
ca	Cathode
D	Destruction
e	Electrical
t	Total/overall

Greek letters

ψ	Exergetic efficiency (%)
η	Thermal/electric efficiency (%)
δ	Thickness (μm)
ρ	Resistivity (Ω m)
ε	Porosity (−)

Abbreviations

BR-BL	Boiler burner
C	Compressor

✉ Shaimaa Seyam
Shaimaa.seyam@ontariotechu.net

Ibrahim Dincer
Ibrahim.dincer@ontariotechu.ca

Martin Agelin-Chaab
Martin.agelin-chaab@ontariotechu.ca

[1] Clean Energy Research Laboratory (CERL), Ontario Tech University, Oshawa, ON L1G 0C5, Canada

CC	Combustion chamber
CFH	Closed feedwater heater
CN	Condenser
D	Desalination
FW	Freshwater
GBC	Gas Brayton cycle
GTHX	Reheater
HP	High pressure
HX	Heat exchanger
LNG	Liquified natural gas
LP	Low pressure
P	Pumps/power
SFC	Specific fuel consumption
SL	Brine
SOFC	Solid oxide fuel cell
SR	Steam reforming
SRC	Steam Rankine cycle
ST	Steam turbine
SW	Seawater
T	Gas turbine
WGS	Water gas shift

Introduction

Large vessels, cargo ships, and oil tankers are the backbone of intercontinental transportation and international commerce. However, environmentalists are worried about their impact on marine ecosystems due to their thermal pollution and greenhouse gas (GHG) emissions [1]. However, GHG emissions are anticipated to rise by 50% in 2050, and an international mitigation governance system is making initiatives to ease some challenges to reducing emissions [2, 3]. An allometric approach is adopted to discover the correlation between ship sizes and speeds and the amount of GHG emissions. It is worth noting that slowing down ship speeds and applying energy-saving strategies can drastically reduce GHG emissions [4]. For example, Ünlügençoğlu et al. [5] collected and monitored emissions from ships and classified the emissions according to ship and engine types. Unfortunately, the emission rates are increased as detected in the Ambarli Port. Also, Muše et al. [6] investigated the emissions from two-stroke marine engine. They found that applying pre-injection method was able to reduce NOx emissions by 9% and reduce the engine efficiency because of the utility of fossil fuels. This raises awareness about marine pollution and encourages many academics and industries to develop eco-friendly ideas to reduce the environmental impact of marine transportation. Therefore, two emission regulations, namely International Maritime Organization Data Collection System and European Union Monitoring, Recording, and Verification, have become essential for ships above 5000 GRT (gross register tonnage) to inspect the carbon emissions in addition to applying energy efficiency management systems [7].

To mitigate the impact of marine transportation on the environment, two possible approaches are worth considering: applying new technology and design for marine engines and utilizing eco-friendly fuels. Vedachalam et al. [8] and Ampah et al. [9] have reviewed marine regulations to restrict the sulfur contents in marine fuels such as distillate marine fuels (DM), ultra-low sulfur fuel oil (ULSFO-DM), residual marine fuel (RM), and high-sulfur heavy fuel oil (HSHFO). They also discussed the role of the international marine organization (IMO) in lowering the border of carbon emissions, nitrogen oxides, sulfur oxides, and particulate matter. Some combinations and processing can be performed for marine fuels; hence, alternative fuels can be introduced and have the potential for better propulsion and power performance, such as hydrogen, liquified natural gas, alcohol fuels (i.e., ethanol and methanol), hydrocarbons (i.e., dimethyl ether), ammonia, and biodiesel and biofuels with the addition of nanoparticles on biodiesel–diesel blends to reduce emissions [10].

Some studies have implemented a combination of Rankine cycles with marine diesel or dual engines. For example, Hountalas et al. [11] combined a Rankine bottoming cycle with the exhaust of a marine diesel engine to utilize waste energy. This integration increases the net power and the overall efficiency and reduces fuel consumption. Aghdoudchaboki et al. [12] combined an organic Rankine cycle and a multi-effect desalination unit with a marine diesel engine to recover the waste heat. The integrated engine can produce a net power of about 390 kW and 7 $m^3\ h^{-1}$ of freshwater, and it has maximum exergy efficiency of 36%. Jafarzad et al. [13] introduced a topping cycle and two bottoming cycles to be combined with the marine diesel engine in order to recover waste heat. The topping cycle is a steam turbocharger, and the bottoming cycles are an organic Rankine cycle (ORC) and reverse-osmosis desalination unit. The overall performance was raised to 82% and 54% thermal and exergetic efficiencies, respectively, and the cogenerated engine can generate a net electric power of 668 kW and a heating load of 650 kW. A similar study was conducted by Pallis et al. [14] by integrating ORC with the heat recovery of a water cooling jacket. Ahn et al. [15] investigated a marine engine involving a combined gas turbine and a steam Rankine cycle operated by liquified natural gas (LNG). They also presented two configurations: one with the same design using liquid hydrogen mixed with LNG, and molten carbonate fuel cell is replaced with a gas turbine and combined with a steam Rankine cycle (SRC). The original design can produce a net power of 65,249 kW with a thermal efficiency of 54.4%, but the first and second configurations can generate 65,792 kW and 65,593 kW, respectively, with an efficiency 53.9%. The first configuration has reduced carbon emissions by 17%

compared to the second configuration, which is increased by 5%. Tsougranis and Wu [16] developed a power plant system of a vessel consisting of four dual-fuel engines and two LNG tanks to be connected to a bottom ORC that depends on a cryogenic pump at the affluent of LNG tanks for cooling the condenser. They used one-stage and two-stage ORC. They found that both ORCs can produce a net power more than 400 kW for one-stage and 550 kW for the two-stage ORC, with thermal and exergetic efficiencies of about 28% for one stage and more than 35% for two stage. The cost of this system can be increased due to the heat exchanger and expanders; however, the fuel consumption saving per year is 344285 $/year with a payback of four years.

The diesel engine is still in use despite its low efficiency compared to other powering systems. Therefore, some studies have been conducted to investigate the performance of other powering systems. For instance, Gonca [17] analyzed an SRC containing three turbines, one open and two closed feedwater heaters. He found that pressure is a necessary condition to consider in the design to gain maximum performance. Gude [18] used the engine exhaust's waste energy to desalinate the ships' ballast water to produce 1000 m^3 day^{-1} freshwater that is sufficient for 2000–4000 occupants. Also, Singh [19] combines a gas turbine cycle with an SRC by using a recovery heat exchanger for steam generation. The thermal efficiency of this combination ranges from 38 to 33% according to the excess air in the combustion of natural gas.

Some state-of-the-art powering systems have been introduced to marine transportation. For example, Long et al. [20] designed hydrogen gas production by utilizing the exhaust gases of a diesel engine that operated using LNG. The process can produce a maximum hydrogen concentration of about 13%, and the thermal efficiency of a steam reformer (SR) ranges from 63 to 94%, according to the amount of excess air. Lion et al. [21] studied a two-stroke marine diesel engine of 13.6 MW. They found a massive amount of waste heat is rejected to the atmosphere. Therefore, they designed SRC and ORC to recapture two energy sources: the high heat of exhaust to the boiler and the rejected heat of condensers by using seawater. The first scenario is SRC and ORC, and the second scenario is only ORC. The first scenario can produce 848 kW, while the second can give 678 kW. This shows the combination of two cycles is a better choice than the other. Chitgar et al. [22] combined a solid oxide fuel cell (SOFC) with freshwater desalination by reverse osmosis process, and they selected methane for hydrogen production from a fuel cell. The combined system can produce a net power of 1.3 MW and about 230 m^3 day^{-1} of freshwater with an exergetic rate of 54%.

As mentioned earlier, marine diesel engines are still operated using diesel fuel with some additives such biodiesel, natural gas, or hydrogen. However, marine engines operated completely with green fuels have not been extensively explored. Therefore, this research is presented to fill this gap. The novelty of the current research is stated as follows:

- The current study presents a new design of marine engine depending on steam Rankine cycle, instead of diesel engine
- The new engine is combined with other powering system, such as fuel cell, gas turbine, and an energy recovery system, such as desalination, to increase the engine performance.
- The new marine engine is fully operated using ecofriendly fuels with different blend combination.

Hence, the specific research objectives are fivefold, namely: (1) to propose a new powering system for marine transport, especially for tankers using a marine steam Rankine cycle and hybridized marine gas turbine; (2) to integrate the proposed engine with a multi-effect desalination to recover the waste heat; (3) to analyze the new engine thermodynamically to assess engine performance; (4) to use five alternative fuels, such as hydrogen, methane, methanol, ethanol, and dimethyl ether, instead of marine gas oil (MGO-DMA). These five fuels are constituents of five hydrogen-based fuel blends; and finally (5) to establish a comparison between the conventional marine engine and the proposed new design to assess the design makers for the best choices.

System description

The proposed new hybrid compound marine engine consists of a regenerative steam Rankine cycle (SRC), a reheat gas Brayton cycle (GBC) and a solid oxide fuel cell (SOFC), as displayed in Fig. 1. The first system is GBC [23], where the air is compressed by a low-pressure compressor (LP-C1), cooled by an intercooler (IC), and compressed again through a high-pressure compressor (HP-C2). Then, a bypass from the compressor air is used for the SOFC system, and the remaining is used for combustion with a fuel blend in the combustion chamber (CC). The SOFC system electrochemically reacts the compressed air with hydrogen produced from the steam reforming and water gas shift of fuel blends to produce electric power. At the same time, the exhaust of SOFC flows to the CC to complete the combustion. The exhaust of CC is used to reheat the outgoing flow of the HP-T1 by a reheater (GTHX) before re-entering the HP-T1. After that, the exhaust gas is expanded again by the LP-T2 and a power turbine (P-T3), which are used in the combustion process of the boiler burner (BR-BL) of the SRC. The specifications of the GBC engine are described in "Brayton gas turbine cycle modelling" section.

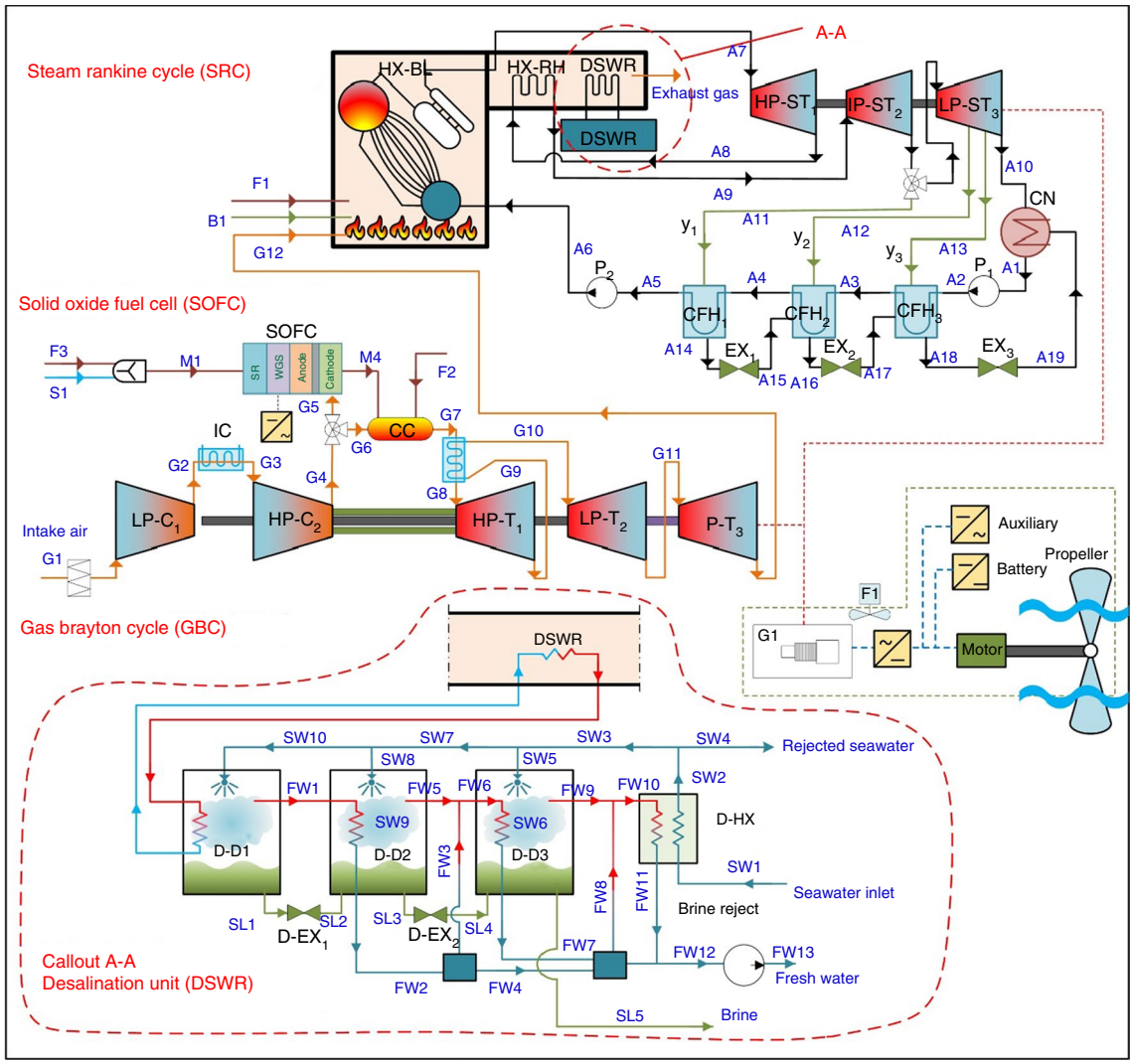

Fig. 1 Schematic diagram of the proposed hybrid combined marine engine

The second system is the SRC, where the water is pumped to the heat exchanger boiler (HX-BL) to be heated to superheated steam with high pressure. The superheated steam is expanded by a high-pressure turbine (HP-ST1), reheated in the boiler, and then expanded again by an intermediate-pressure turbine (IP-ST2). After that, the steam exits the IP-ST2 and splits into two pathways: to the third closed feedwater heater (CFH3) and to the low-pressure turbine (LP-ST3) to be expanded to very low pressure of the condenser (CN). There are two steam bleeds from the LP-ST3 and one steam bleed from the IP-ST2 that flow to closed feedwater heaters (CFH) and exist to a trap to drop the pressure to the affluent device.

Therefore, the first CFH1 receives a steam bleed to be cooled and expelled to a trap (EX3) to the condenser. The second CFH2 receives a steam bleed at different pressure and exits to the second CFH2 through (EX2). The last one obtains a steam bleed at different pressure and ejects to the third CFH3 through a trap of (EX1). The burner boiler is employed to combust the remaining fuel blend from the GBC with the fuel blend of F1 and air of B1 streams. The exhaust gases inside the boiler are used to heat the pressurized water from A6 to superheated steam of A7 using the boiler heat exchanger HX-BL before the turbine inlet and heat the steam of reheater in HX-RH. Also, the waste heat is used for seawater desalination unit (DSWR) to produce freshwater for an Aframax ship.

The ship propeller is operated using a generator fed by the electric power generated from the SRC, GBC, and SOFC. Since the ship runs at different speeds with different loads, any excess electric power can be used for any auxiliary system, such as lighting, air-conditioning, and emergency generators, and the remaining unwanted power can be stored using batteries.

Table 1 Specification of a tanker ship and its engine for marine transportation [24, 25]

Ship specifications	Value
Ship model	Aframax WSD 42 111 k
Ship type	Tanker for oil and products
Length overall	252.80 m
Deadweight, max. draft	111,000 DWT
Service speed	14.5 knots
Cargo segregation	12 cargo tanks
Fuel oil consumption	35.2 t day^{-1}
Generator sets	3 × 875 kWe
Emerg./harbor generator	1 × 200 kWe
Engine	2-Stoke Wartsila 6 × 62 for 10,400 kW
Engine output power	15,960 kW
Engine weight	377 ton

The selected ship is an Aframax oil tanker used for transporting refined or unrefined oil on the east coast of Canada. It has a length of 254 m and a maximum 120,000 DWT, and it can carry up to 4 million barrels of oil. The specifications of this ship and its engine are displayed in Table 1. The aframax engine is a two-stroke ICE engine with a turbocharger; however, it will be replaced by a steam Rankine cycle to produce the same power of 15,960 kW using marine gas oil (MGO-DMA), which comprises 75% saturated hydrocarbons containing paraffin and naphthenes, 24% unsaturated hydrocarbons as benzene rings, 1% Asphaltenes. The properties of MGO-DMA are presented in Table 2. The alternative fuels are selected as hydrogen, methanol, ethanol, dimethyl-ether (DME), and methane to substitute the MGO-DMA; their properties are also shown in Table 2. In addition, the stoichiometric combustion reactions for all fuels are mentioned in Table 3.

System modeling

The hybrid combined marine engine is modeled using thermodynamic analysis and simulated using Aspen PLUS. This software program is a reliable and established software in the field of thermo-chemical engineering. A separate component represents each engine process to present a closer approach to reality, which will be explained later.

Steam Rankine cycle modeling

The regenerative steam Rankine cycle contains three turbines (HP-ST1, IP-ST2, and LP-ST3), a condenser (CN), two

Table 2 Specifications of fuels for developed marine transportation systems

Specifications	MGO-DMA [26, 27]	Hydrogen [28]	Methanol [29]	Ethanol [30]	DME [31]	Methane [32]
Molecular formula	–	H_2	CH_3OH	CH_3OHCH_2	CH_3OCH_3	CH_4
Molecular weight /kg $kmol^{-1}$	220–238	2.016	46.069	46.07	46.07	16.043
Adiabatic flame temperature /°C	2101	2000	1949	2082	2100	1963
Auto-ignition temperature /°C	256	571	470	365	350	537
Density at 40 °C /kg m^{-3}	815–870	0.0773	792	789	2.11	0.657
Viscosity at 40 °C/mm^2 s^{-1}	4.5	109	0.75	1.056	0.184	18.72
High heating value /MJ kg^{-1}	45.9	141.9	22.7	29.7	31.67	55.5
Low heating value /MJ kg^{-1}	42.8	119.0	18.1	26.7	28.87	50

Table 3 Stoichiometric combustion reactions for the fuels

Fuel	Stoichiometric combustion reaction	Heat of combustion (ΔHc), kJ mol^{-1}
MGO-DMA	Paraffins (C_nH_{2n+2}): $C_6H_{14} + 9.5\ O_2 \rightarrow 6\ CO_2 + 7\ H_2O$	− 10,557
	Naphthenes (C_nH_{2n}): $C_6H_{12} + 9\ O_2 \rightarrow 6\ CO_2 + 6\ H_2O$	
	Aromatics (C_6H_6): $C_6H_6 + 7.5\ O_2 \rightarrow 6\ CO_2 + 3\ H_2O$	
	Asphalates (C_7H_8): $C_7H_8 + 9\ O_2 \rightarrow 7\ CO_2 + 4\ H_2O$	
Hydrogen	$2\ H_2 + O_2 \rightarrow 2\ H_2O$	− 286
Methanol	$CH_3OH + 1.5\ O_2 \rightarrow CO_2 + 2\ H_2O$	− 726
Ethanol	$CH_3OHCH_2 + 3\ O_2 \rightarrow 2\ CO_2 + 3\ H_2O$	− 1366.91
DME	$CH_3OCH_3 + 3\ O_2 \rightarrow 2\ CO_2 + 3\ H_2O$	− 2726.3
Methane	$CH_4 + 2\ O_2 \rightarrow CO_2 + 2\ H_2O$	− 891

pumps (P1 and P2), three closed feedwater heaters (CFH1 to CFH3) accompanied with their expansion valves (EX1, EX2, and EX3), and a heat exchanger boiler (HXBL), a reheater (HXRH), and a desalination unit (DSWR). The condenser (CN) is a shell and tube heat exchanger using seawater for cooling media that is pumped from the sea and rejected back to the sea. The specifications of SCR are listed in Table 4. The resultant power of this system is evaluated as follows:

$$\dot{W}_{\mathrm{SRC}} = \dot{W}_{\mathrm{HPST1}} + \dot{W}_{\mathrm{IPST2}} + \dot{W}_{\mathrm{LPST3}} - \left(\dot{W}_{\mathrm{P1}} + \dot{W}_{\mathrm{P2}}\right) \tag{1}$$

The power of the low-pressure turbine is a function of the bleeding mass fraction to the closed feedwater heaters, which are equal amount and can be given as y. Therefore, the LP-ST3 is written as:

$$\begin{aligned}\dot{W}_{\mathrm{LPST3}} = {} & \dot{m}_{\mathrm{ST}}(1-y)\left(h_{\mathrm{A11}} - h_{\mathrm{A12}}\right) \\ & + \dot{m}_{\mathrm{ST}}(1-2y)\left(h_{\mathrm{A12}} - h_{\mathrm{A13}}\right) \\ & + \dot{m}_{\mathrm{ST}}(1-3y)\left(h_{\mathrm{A13}} - h_{\mathrm{A10}}\right)\end{aligned} \tag{2}$$

The feedwater heaters have an energy balance as indicated below:

$$\text{CFH1} \quad y\dot{m}_{\mathrm{ST}}\left(h_{\mathrm{A11}} - h_{\mathrm{A14}}\right) = \dot{m}_{\mathrm{ST}}\left(h_{\mathrm{A5}} - h_{\mathrm{A4}}\right) \tag{3}$$

$$\text{CFH2} \quad y\dot{m}_{\mathrm{ST}}h_{\mathrm{A12}} + y\dot{m}_{\mathrm{ST}}h_{\mathrm{A15}} - 2y\dot{m}_{\mathrm{ST}}h_{\mathrm{A16}} = \dot{m}_{\mathrm{ST}}\left(h_{\mathrm{A4}} - h_{\mathrm{A3}}\right) \tag{4}$$

$$\text{CFH3} \quad y\dot{m}_{\mathrm{ST}}h_{\mathrm{A13}} + y\dot{m}_{\mathrm{ST}}h_{\mathrm{A17}} - 3y\dot{m}_{\mathrm{ST}}h_{\mathrm{A18}} = \dot{m}_{\mathrm{ST}}\left(h_{\mathrm{A3}} - h_{\mathrm{A2}}\right) \tag{5}$$

The required heat of exchanger boiler (HXBL) and reheater (HXRH) are calculated as the following:

$$\dot{Q}_{\mathrm{HXBL}} = \dot{m}_{\mathrm{ST}}\left(h_{\mathrm{A7}} - h_{\mathrm{A6}}\right) \tag{6}$$

$$\dot{Q}_{\mathrm{HXRH}} = \dot{m}_{\mathrm{ST}}\left(h_{\mathrm{A9}} - h_{\mathrm{A8}}\right) \tag{7}$$

Another heat exchanger is added to the exhaust gases at the chimney to use the waste energy in the desalination unit of (DSWR) to desalinate the seawater and produce freshwater for the ship, which will be explained in a separate section. The useful heat of DSWR is a function of exhaust gas flow rate, $\dot{m}_{\mathrm{B4}}$ (see Fig. 3) and the difference of specific enthalpy between the inlet and exit flow of h_{B4} and h_{B5}, respectively, which is written as follows:

$$\dot{Q}_{\mathrm{DSWR}} = \dot{m}_{\mathrm{B4}}\left(h_{\mathrm{B4}} - h_{\mathrm{B5}}\right) \tag{8}$$

The boiler is heated by burning a fuel blend with air mixed with the exhaust of gas Brayton cycle of G12 stream. The input heat of fuel combustion in the burner (BRBL) is estimated as follows:

$$\dot{Q}_{\mathrm{BRBL}} = \dot{m}_{\mathrm{B2}}h_{\mathrm{B2}} - \left(\dot{m}_{\mathrm{F1}}h_{\mathrm{F1}} + \dot{m}_{\mathrm{B1}}h_{\mathrm{B1}} + \dot{m}_{\mathrm{G12}}h_{\mathrm{G12}}\right) \tag{9}$$

The required power of the two pumps of P1 and P2 is calculated below:

$$\dot{W}_{\mathrm{P1}} = \eta_{\mathrm{P1}}\dot{m}_{\mathrm{ST}}v_{\mathrm{A1}}\left(P_{\mathrm{A2}} - P_{\mathrm{A1}}\right) \tag{10}$$

$$\dot{W}_{\mathrm{P2}} = \eta_{\mathrm{P2}}\dot{m}_{\mathrm{ST}}v_{\mathrm{A5}}\left(P_{\mathrm{A6}} - P_{\mathrm{A5}}\right) \tag{11}$$

The performance of SRC is evaluated using energetic efficiency, η_{SRC}, and exergetic efficiency, ψ_{SRC}, as below:

$$\eta_{\mathrm{SRC}} = \frac{\dot{W}_{\mathrm{SRC}} + \dot{Q}_{\mathrm{DSWR}}}{\dot{Q}_{\mathrm{BRBL}}} \quad \text{and} \quad \psi_{\mathrm{SRC}} = \frac{\dot{W}_{\mathrm{SRC}} + \dot{E}x^{Q}_{\mathrm{DSWR}}}{\dot{E}x^{Q}_{\mathrm{BRBL}}} \tag{12}$$

Table 4 Specifications of SCR

Parameter	Value
Steam mass flow rate	6 kg s^{-1}
Maximum temperature before first turbine	536.9 °C
Reheater temperature	526.9 °C
Maximum pressure	7100 kPa
Turbine exit pressures	1700 kPa, 1000 kPa, 5 kPa
Turbine and pump thermal efficiency	85%
Turbine and pump mechanical efficiency	90%
Minimum pressure	5 kPa
First pump pressure ratio	5
Second pump pressure ratio	14.2
Steam bleeding ratio for all CFH	0.1
Steam bleeding pressures	1000 kPa, 600 kPa, and 300 kPa
Condenser cooling media	Seawater enters at 15 °C and 500 kPa and leaves at 21 °C and 500 kPa

Table 5 Specifications of marine gas turbine engine [33]

Specifications	Values
Gas turbine model	Taurus 60
Output power	Up to 5740 kW (7700 hp)
Turbine and compressors thermal efficiency	85%
Turbine and compressors mechanical efficiency	90%
Maximum speed	15,000 rpm
Dimension	6 m (L) × 2.5 m (W) × 2.7 m (H)
Mass	15,420 kg (34,000 lb)

Brayton gas turbine cycle modeling

The marine gas Brayton cycle (GBC) is selected to be Taurus 60 [33], with specifications presented in Table 5. It consists of low- and high-pressure compressors (LP-C1 and HP-C2), an intercooler (IC), a combustion chamber (CC), two turbines (HP-T1 and LP-T2), a reheater (GTHX), and a power turbine (P-T3). This configuration is to reduce the back work ratio (compressors' power to turbines' power) and increase the GBC efficiency. The net power of GBC is determined as the summation of all turbine power minus the summation of all compressor power as written below:

$$\dot{W}_{\mathrm{GBC}} = \dot{W}_{\mathrm{HPT1}} + \dot{W}_{\mathrm{LPT2}} + \dot{W}_{\mathrm{PT3}} - \dot{W}_{\mathrm{LPC2}} - \dot{W}_{\mathrm{HPC3}} \tag{13}$$

The resultant required heat of GBC is given as follows:

$$\dot{Q}_{\mathrm{GBC}} = \dot{Q}_{\mathrm{CC}} - \dot{Q}_{\mathrm{IC}} \tag{14}$$

The energetic and exergetic efficiencies that can evaluate the performance of GBC are below:

$$\eta_{\mathrm{GBC}} = \frac{\dot{W}_{\mathrm{GBC}}}{\dot{Q}_{\mathrm{GBC}}} \quad \text{and} \quad \psi_{\mathrm{GBC}} = \frac{\dot{W}_{\mathrm{GBC}}}{\dot{E}x^{Q}_{\mathrm{CC}} - \dot{E}x^{Q}_{\mathrm{IC}}} \tag{15}$$

Solid oxide fuel cell system

One cell of SOFC comprises two porous anodic electrodes (Ni–ZrO_2 or Co–ZrO_2 cermet), two porous cathodic electrodes (strontium-doped lanthanum manganate ($LaMnO_3$)), and an oxide-ion conducting electrolyte (yttria stabilized with zirconia) [34]. Air enters the cathodic electrode and produces oxygen ions that are transferred to the anodic electrode to react with hydrogen and hence generate electricity through electrons as well as steam. Also, a fuel blend is mixed with water, and both enter the direct SOFC that involves in two stages: steam reforming (SR) and water gas shift (WGS). They are essential stages to deal with different hydrocarbon fuels, not only methane, to produce hydrogen gas at the anode. The specific data details of SOFC are outlined in Table 6, along with the electrochemical reactions of the SOFC as given below:

- At anode side: $H_2 + O^{2-} \rightarrow H_2O + 2\,e^-$
- At cathode side: $0.5\,O_2 + 2e^- \leftrightarrow O^{2-}$
- Overall: $H_2 + 0.5\,O_2 \leftrightarrow H_2O$

Table 7 provides the specific equations about cell voltage and potential losses in the SOFC. The electric power of SOFC is then expressed as follows:

$$\dot{W}_{\mathrm{SOFC}} = \eta_{\mathrm{inv}} i A_{\mathrm{t}} V_{\mathrm{c}} \tag{16}$$

where η_{inv} denotes for efficiency of an inverter (95%). The overall SOFC electric efficiency, $\eta_{\mathrm{SOFC,e}}$, is defined as the ratio of the cell voltage to the Nernst voltage. The change of cell volage versus the current density is illustrated in Fig. 2 at 1073 K and 1823 kPa. The SOFC is operated at 0.6 A cm^{-2}, which is located on the linear relationship of ohmic loss far from the activation loss and concentration loss, as shown in Fig. 2. This validates the selection of the current density and the cell voltage of SOFC.

The thermal and exergetic efficiency of SOFC is indicated as $\eta_{\mathrm{SOFC,th}}$ and ψ_{SOFC}, respectively. They depend particularly on the added heat of SOFC, $\dot{Q}_{\mathrm{SOFC}}$, which is given as the summation of the heat terms in the SOFC due to the

Table 6 Datasheet of SOFC [35]

Parameters	Value
Cell temperature, T_c /K	1073
Cell pressure, P_c /kPa	1823
Current density, i /A/ m^{-2}	6000
Active cell area, A_c /m^2	0.7
# of cells per a stack, Nc	100
# of stacks, Ns	34
Total area, A_t/m^2	2380
Anode thickness, δ_{an}/μm	20
Cathode thickness, δ_{ca}/μm	50
Electrolyte thickness, δ_{el}/μm	500
Interconnect thickness, δ_{in} /μm	20
Porosity of anode, ε_{na}	0.5
Porosity of cathode, ε_{ca}	0.5
Tortuosity for anode and cathode, ξ	6
FDV* of hydrogen, ν_{H_2} /m^3	7.07
FDV* of water, ν_{H_2O}/m^3	12.7
FDV* of oxygen, ν_{O_2}/m^3	16.6
FDV* of nitrogen, ν_{N_2}/m^3	17.9

*FDV… Fuller diffusion volume

Table 7 Modeling the SOFC [36, 37]

Cell voltage:	
$V_c = E_N - \eta_{act} - \eta_\Omega - \eta_{con}$	
Nernst voltage:	$E_N = -\frac{\Delta \bar{g}}{2F} - \frac{\bar{R}T_c}{2F}\ln\left(\frac{p_{H_2O}}{p_{H_2}\sqrt{p_{O_2}}}\right)$
Activation loss:	
$\eta_{act} = \eta_{act,an} + \eta_{act,ca}$	
By anode:	$\eta_{act,an} = \frac{\bar{R}T_c}{2\alpha_{an}F}\sinh^{-1}\left(\frac{i}{2i_{0,an}}\right)$
Exchange current density of anode:	$i_{0,an} = \gamma_{an}\left(\frac{P_{H_2}}{P_{ref}}\right)\left(\frac{P_{H_2O}}{P_{ref}}\right)\exp\left(-\frac{E_{act,an}}{\bar{R}T_c}\right)$
Pre-exponential coefficient for anode:	$\gamma_{an} = 7\times10^9\ \mathrm{A\ m^{-2}}$
By cathode:	$\eta_{act,ca} = \frac{\bar{R}T_c}{2\alpha_{ca}F}\sinh^{-1}\left(\frac{i}{2i_{0,ca}}\right)$
Exchange current density of cathode:	$i_{0,ca} = \gamma_{ca}\left(\frac{P_{O_2}}{P_{ref}}\right)^{0.25}\exp\left(-\frac{E_{act,ca}}{\bar{R}T_c}\right)$
Pre-exponential coefficient for cathode:	$\gamma_{ca} = 2\times10^9\ \mathrm{A\ m^{-2}}$
Ohmic loss:	
$\eta_\Omega = \frac{i\left(\rho_{an}\delta_{an}+\rho_{ca}\delta_{ca}+\rho_{el}\delta_{el}+\rho_{in}\delta_{in}\right)}{A_c}$	
Specific material resistivity:	$\rho_{an} = 2.98\times10^{-5}\exp\left(-\frac{1392}{T_c}\right)$
	$\rho_{ca} = 8.114\times10^{-5}\exp\left(\frac{600}{T_c}\right)$
	$\rho_{el} = 2.94\times10^{-5}\exp\left(\frac{10{,}350}{T_c}\right)$
	$\rho_{in} = 1.257\times10^{-5}\exp\left(\frac{4690}{T_c}\right)$
Concentration loss:	
$\eta_{con} = \eta_{con,an} + \eta_{con,ca}$	
By anode:	$\eta_{con,an} = -\frac{\bar{R}T_c}{2F}\ln\left(1-\frac{i}{i_{L,an}}\right) + \frac{\bar{R}T}{2F}\ln\left(1+\frac{P_{H_2}i}{P_{H_2O}i_{L,an}}\right)$
Limiting current density of anode:	$i_{L,an} = \frac{2FP_{H_2}D_{an(eff)}}{\bar{R}T_c}$
By cathode:	$\eta_{con,ca} = -\frac{\bar{R}T_c}{2F}\ln\left(1-\frac{i}{i_{L,ca}}\right)$
Limiting current density of cathode:	$i_{L,ca} = \frac{2FP_{O_2}D_{ca(eff)}}{\bar{R}T_c}$
Effective diffusivity:	
Ordinary diffusion coefficient:	$D_{O,ik} = \frac{1\times10^{-7}T^{1.25}\left(M_i^{-1}+M_k^{-1}\right)^{0.5}}{P\left(v_i^{1/3}+v_k^{1/3}\right)}$
Effective ordinary diffusion coefficient:	$D_{O,i(eff)} = D_{O,i}\left(\frac{\varepsilon}{\xi}\right)$
Knudsen diffusion coefficient:	$D_{K,i} = 97r\sqrt{\frac{T}{M_i}}$
Effective Knudsen diffusion coefficient:	$D_{K,i(eff)} = D_{K,i}\left(\frac{\varepsilon}{\xi}\right)$
Overall diffusion coefficient:	$\frac{1}{D_{i(eff)}} = \frac{1}{D_{K,i(eff)}} + \frac{1}{D_{O,i(eff)}}$
Effective diffusivity of anode:	$D_{an(eff)} = \left(\frac{P_{H_2O}}{P_{an}}\right)D_{H_2(eff)} + \left(\frac{P_{H_2}}{P_{an}}\right)D_{H_2O(eff)}$
Effective diffusivity of cathode:	$D_{ca(eff)} = D_{O_2(eff)}$

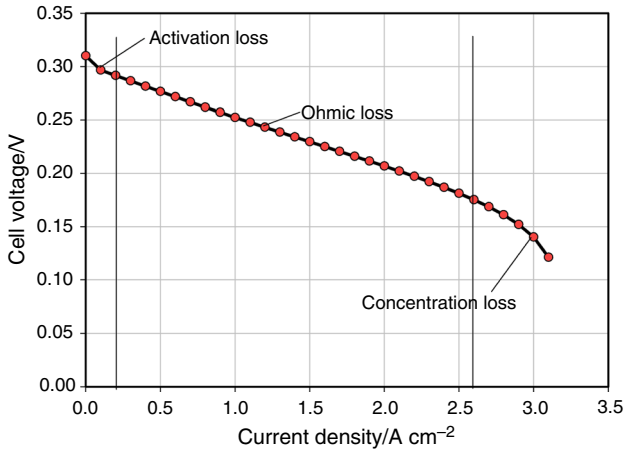

Fig. 2 Polarization curve of SOFC at 1073 K and 1823 kPa

chemical reaction of anode and cathode minus the heat of SR and WSG:

$$\eta_{\mathrm{SOFC,e}} = \frac{V_{\mathrm{c}}}{E_{\mathrm{N}}} \tag{17}$$

$$\eta_{\mathrm{SOFC,th}} = \frac{\dot{W}_{\mathrm{SOFC}}}{\dot{Q}_{\mathrm{SOFC}}} \quad \text{and} \quad \psi_{\mathrm{SOFC}} = \frac{\dot{W}_{\mathrm{SOFC}}}{\dot{E}x^{Q}_{\mathrm{SOFC}}} \tag{18}$$

Note that the sustainable fuels previously mentioned in Table 2 form five fuel blends with hydrogen as the basis, as shown in Table 8, which are named MF#. The mass ratios and the total high and low heating values of five fuel blends are given in Table 8, along with the chemical reactions in the steam reformer (SR) and water gas shift (WGS) reactor, accordingly. The average fuel HHV and LHV is 71.5 MJ kg^{-1} and 61.1 MJ kg^{-1}, respectively, which are greater than that of MGO-DMA, as shown in Table 2. That means these fuel selections can have less mass flow rate for the same combustion heat resulting in high engine performance. The fuel blends in this study are modeled as complete combustion with excess air of 25% in the CC and 4% in the BRBL, so that equivalence ratio of combustion is around 0.7 in the CC and 0.95 in the BRBL, which helps the excess air still flows to the BRBL from the GBC and continues to combust the fuel in the BRBL as well.

Desalination unit (DSWR)

The multi-effect desalination system (DSWR) consists of three stages (D-D#) under the same temperature difference. The brine temperature, T_{i}, is decreased for the next unit by the temperature difference

$$\Delta T = \frac{T_{\mathrm{D-D1}} - T_{\mathrm{D-D3}}}{3-1} \tag{19}$$

The condensation temperature inside each stage is the difference between the brine temperature and the boiling point elevation (BPE). The feed seawater flow rate,$\dot{m}_{\mathrm{SW}}$, is equally distributed to all stages. A constant salinity of seawater x_{i} is assumed throughout all effects. The brine leaving stage (i), $\dot{m}_{\mathrm{SLi}}$, is introduced into the next stage ($i+1$). Therefore, the pure water, $\dot{m}_{\mathrm{FWi}}$, leaves the stage and heats the next stage. This is repeated until the last stage has no salinity. The mass flow rate of desalinated water, $\dot{m}_{\mathrm{FWi}}$, is calculated as:

$$\dot{m}_{\mathrm{FWi}} = \sum_{\mathrm{k=1}}^{i} \dot{m}_{\mathrm{SWi}} - \dot{m}_{\mathrm{SLi}} \tag{20}$$

Table 8 Mass ratios, heating values, and chemical reactions of the presently considered fuel options

Fuels	Mass ratio					HHV[MJ kg^{-1}]	LHV[MJ kg^{-1}]	SR	WGS
	H_2	CH_4	CH_3OH	CH_3OHCH_2	CH_3OCH_3				
MF1	0.25	0.75	0	0	0	77.1	67.3	$CH_4+H_2O\rightarrow CO+3\,H_2$	$CO+H_2O\rightarrow CO_2+H_2$
MF2	0.25	0	0.75	0	0	52.5	43.3	$CH_3OH\rightarrow CO+2\,H_2$	$CO+H_2O\rightarrow CO_2+H_2$
MF3	0.40	0	0	0.60	0	74.6	63.6	$CH_3OHCH_2\rightarrow CH_4+CO+H_2$ $CH_4+H_2O\rightarrow CO+3\,H_2$	$CO+H_2O\rightarrow CO_2+H_2$
MF4	0.40	0	0	0	0.60	75.8	64.9	$CH_3OCH_3\rightarrow CH_4+CO+H_2$ $CH_4+H_2O\rightarrow CO+3\,H_2$	$CO+H_2O\rightarrow CO_2+H_2$
MF5	0.40	0.15	0.15	0.15	0.15	77.7	66.2	$CH_4+H_2O\rightarrow CO+3\,H_2$ $CH_3OH\rightarrow CO+2\,H_2$ $CH_3OHCH_2\rightarrow CH_4+CO+H_2$ $CH_3OCH_3\rightarrow CH_4+CO+H_2$	$CO+H_2O\rightarrow CO_2+H_2$

The first stage can be analyzed thermodynamically by estimating the mass balance, partial mass balance, and the energy balance equations, as indicated below:

$$\dot{m}_{\mathrm{FW},1} = \dot{m}_{\mathrm{SW},1} - \dot{m}_{\mathrm{SL},1} \tag{21a}$$

$$x_{\mathrm{SW}}\dot{m}_{\mathrm{SW}} = x_{\mathrm{SL}}\dot{m}_{\mathrm{SL}} = x_{\mathrm{SL}}\left(\dot{m}_{\mathrm{SW}} - \dot{m}_{\mathrm{FW}}\right) \tag{21b}$$

$$\dot{Q}_{\mathrm{DSWR}} = \dot{m}_{\mathrm{s}}c\left(T_{\mathrm{s,in}} - T_{\mathrm{s,ex}}\right) \tag{21c}$$

$$\dot{Q}_{\mathrm{DSWR}} = \dot{m}_{\mathrm{FW},1}h_{\mathrm{fg},1} + \dot{m}_{\mathrm{SW},1}c\left(T_1 - T_{\mathrm{SW}}\right) \tag{21d}$$

The desalinated water is used to heat the next stage, while the brine of the previous stage enters the next one and heats the seawater to remove its salinity. The mass balance and the energy balance equations of the following stages are explained below:

$$\dot{m}_{\mathrm{SL,i}} = \dot{m}_{\mathrm{SW,i}} - \left(\dot{m}_{\mathrm{SL,i}} - \dot{m}_{\mathrm{SL,i-1}}\right) \tag{22a}$$

$$x_{\mathrm{SW}}\dot{m}_{\mathrm{SW}} + x_{\mathrm{SL,i-1}}\dot{m}_{\mathrm{SL,i-1}} = x_{\mathrm{SL,i}}\dot{m}_{\mathrm{SL,i}} \tag{22b}$$

$$\dot{Q}_{\mathrm{s,i}} = \dot{m}_{\mathrm{FW,i-1}}h_{\mathrm{fg,i-1}} + \dot{m}_{\mathrm{SL,i-1}}c_{\mathrm{P}}\left(T_{\mathrm{i-1}} - T_{\mathrm{i}}\right) \tag{22c}$$

$$\dot{Q}_{\mathrm{s,i}} = \dot{m}_{\mathrm{FW,i}}h_{\mathrm{fg,i}} + \dot{m}_{\mathrm{SW,i}}c_{\mathrm{P}}\left(T_{\mathrm{i}} - T_{\mathrm{F}}\right) \tag{22d}$$

The thermal efficiency of the desalination (DSWR), η_{DSWR}, and its exergy efficiency, ψ_{DSWR}, can be described below. Also, the gained output ratio (GOR) is calculated by the ratio of the latent heat of fresh water exiting the last stage to the input heat of steam entering the first stage.

$$\eta_{\mathrm{DSWR}} = \frac{\dot{m}_{\mathrm{FW15}}h_{\mathrm{FW16}}}{\dot{Q}_{\mathrm{DSWR}}} \tag{23}$$

$$\psi_{\mathrm{DSWR}} = \frac{\dot{m}_{\mathrm{FW15}}\mathrm{ex}_{\mathrm{FW16}}}{\dot{E}x^{Q}_{\mathrm{DSWR}}} \tag{24}$$

$$\mathrm{GOR} = \frac{\dot{m}_{\mathrm{FW15}}h_{\mathrm{fg}}}{\dot{Q}_{\mathrm{DSWR}}} \tag{25}$$

Overall performance

The overall performance of the ship engine is defined as the ratio of the useful output energy/exergy rates to the required input energy/exergy rates. The useful energy rates are the net power of the SRC, GBC, and SOFC and the amount of fresh water extracted from the seawater, while the input energy is the fuel combustion in the CC and BRBL and the input of SOFC. The overall energetic and exergetic efficiencies are written below:

$$\eta_{\mathrm{DSWR}} = \frac{\dot{W}_{\mathrm{SRC}} + \dot{W}_{\mathrm{GBC}} + \dot{W}_{\mathrm{SOFC}} + \dot{m}_{\mathrm{FW15}}h_{\mathrm{FW16}}}{\dot{Q}_{\mathrm{CC}} + \dot{Q}_{\mathrm{BRBL}} + \dot{Q}_{\mathrm{SOFC}}} \tag{26}$$

$$\psi_{\mathrm{DSWR}} = \frac{\dot{W}_{\mathrm{SRC}} + \dot{W}_{\mathrm{GBC}} + \dot{W}_{\mathrm{SOFC}} + \dot{m}_{\mathrm{FW15}}\mathrm{ex}_{\mathrm{FW16}}}{\dot{E}x^{\mathrm{Q}}_{\mathrm{CC}} + \dot{E}x^{\mathrm{Q}}_{\mathrm{BRBL}} + \dot{E}x^{\mathrm{Q}}_{\mathrm{SOFC}}} \tag{27}$$

Results and discussion

This section intends to cover the results of a comprehensive analysis and assessment of the presently developed integrated engine system with multiple fuel options using the Aspen Plus. It also discusses the impact of fuel selection on engine performance and some parametric studies to understand engine behavior.

Thermodynamic analysis

A detailed analysis using energy and exergy methods is performed on the hybrid combined marine powering system through the Aspen Plus. The flow chart for the SRC is shown in Fig. 3, and the steam streams are numbered with A#, while the streams of chimney exhaust are numbered with B#. B2 stream is the connection between the SRC and GBC. The flow chart for the GBC is displayed in Fig. 4; its stream numbers are G#, and M# streams are for the SOFC subsystem. Finally, Fig. 5 illustrates the flowchart for the desalination unit (DSWR), which contains three main streams: SW# is for feed and seawater, FW# is for desalinated freshwater, and SL# is for the brine stream. The equations of states are selected to be Soave–Redlick–Kwong (SRK) for the GBC for hydrocarbon mixture and combustion at high pressure and temperature; Peng Robinson for the SRC for steam thermodynamic properties at various pressure and temperature; and ELECNTRL for MED desalination system for modeling brines.

The thermodynamic properties of streams are evaluated and listed in Tables 9, 10 and 11. The steam enters the boiler at A6 of 7100 kPa and 510.1 K and superheats to A7 of 7100 kPa and 810 K, as shown in Table 9. The discharge pressure of turbines is 1700 kPa for HP-ST1, 1000 for IP-ST2, and 5 kPa for LP-ST3. The breeding pressure is 1000 for the CFH1, 600 for the CFH2, and 300 kPa for the CFH3. The steam mass flow rate is 6 kg s^{-1}. The mass fraction of bleeding steam is 10% of the feeder. The condenser pressure is 5 kPa and cools the steams using water at 15 ℃ and 400 kg s^{-1} to be heated to 21.9 ℃. The

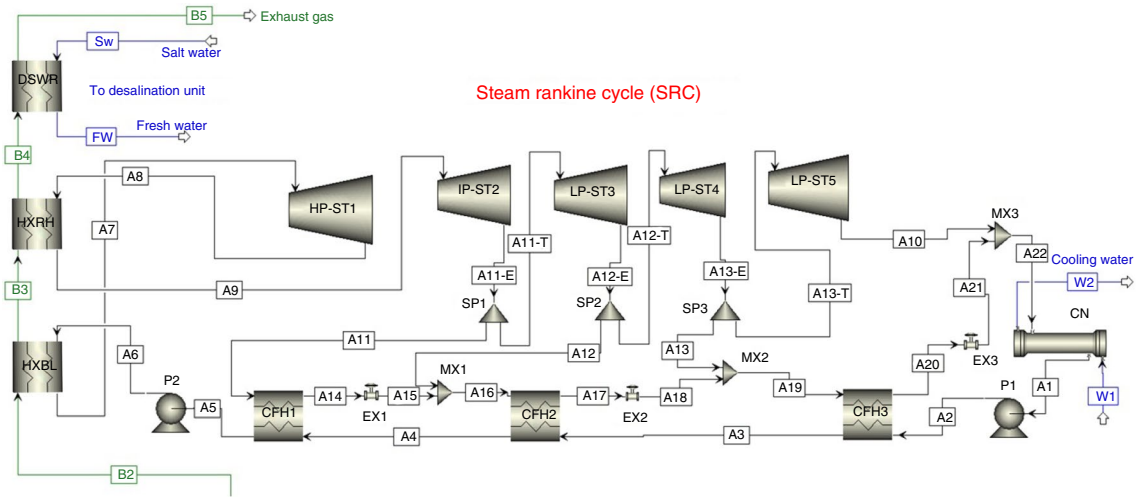

Fig. 3 Aspen Plus flowchart of the SRC. The stream B2 exits from the burner boiler (BR-BL) to the heat exchanger boiler (HXBL) (see Fig. 3)

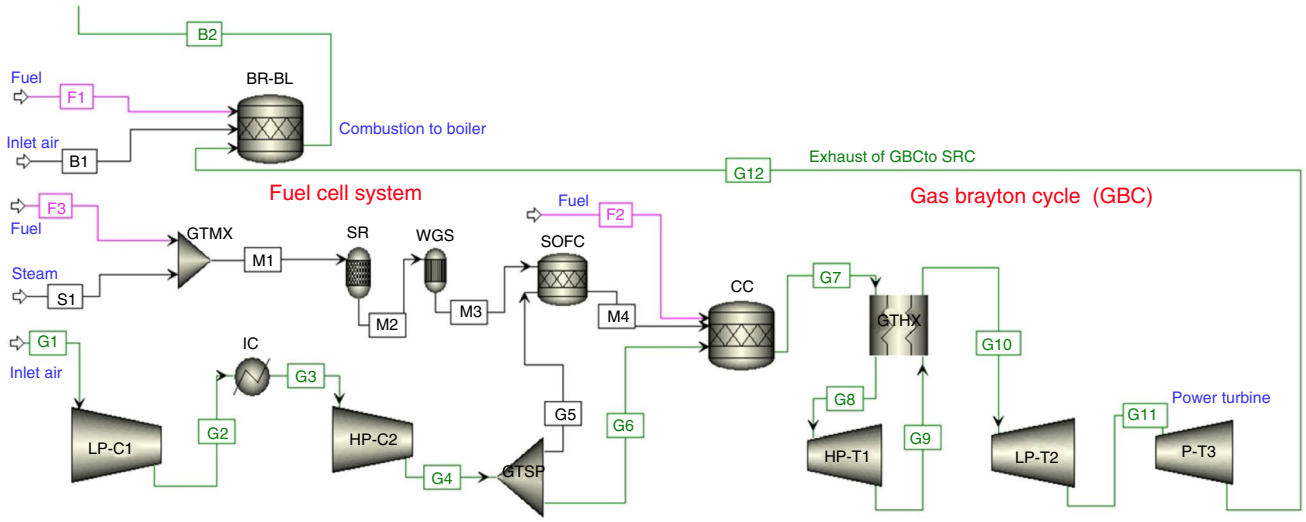

Fig. 4 Aspen Plus flowchart of the hybrid GBC. The stream B2 flows to the heat exchanger boiler (HXBL)

first pump increased the condensed steam from 5 kPa and 37.4 ℃ to 500 kPa and 37.5 ℃, while the second pump increased the saturated liquid to 7100 kPa. The feedwater heaters increase the low-pressure liquid temperature to 86.1 ℃ by CFH3, 136.8 ℃ by CFH2, and 152.7 ℃ by CFH1 to ensure the exit of bleeding steam for the feedwater heaters reach the saturated liquid at their working pressure.

For the GBC, the mass flow rate of intake air of G1 is 30 kg s^{-1} at 25 ℃ and 101.3 kPa, which is pressurized to 429.5 kPa and 1823.2 kPa with an overall pressure ratio of 18, as shown in Table 10. The fuel blend is combusted with air under stoichiometric combustion with excess air at a high temperature of 1200 ℃ and 1823 kPa and then decreased to 1100 ℃ by GTHX for blade safety. The exhaust gases expanded to 750 kPa by HP-T1, 350 kPa by LP-T2, and 200 kPa by P-T3. The exhaust gases are released from the GBC at 730.8 ℃ and 200 kPa of G12 stream to enter the burner boiler (BRBL). The mass flow rate of G5 is 6 kg s^{-1} which is 20% of the intake air. The fuel blend and water mass flow rates of F3 and S1 are 0.25 kg s^{-1} and 0.4 kg s^{-1}. The fuel mixture enters the direct SOFC system to be reformed at 200 ℃, then water shifted at 400 ℃, and electrochemically reacted with air at 800 ℃. The fuel blend, 25 mass% hydrogen and 75 mass% methane, is 1 kg s^{-1} at F2 and 0.2 kg s^{-1} at F1, while the intake air of B1 is 0.5 kg s^{-1}. Finally, the exhaust gases at B5 flow at 32.35 kg s^{-1} with 216 ℃ and 200 kPa.

The desalination unit (DSWR) uses the seawater with a salinity of 0.035 kg kg^{-1} at 12 ℃ and 105 kPa at SW1 to be

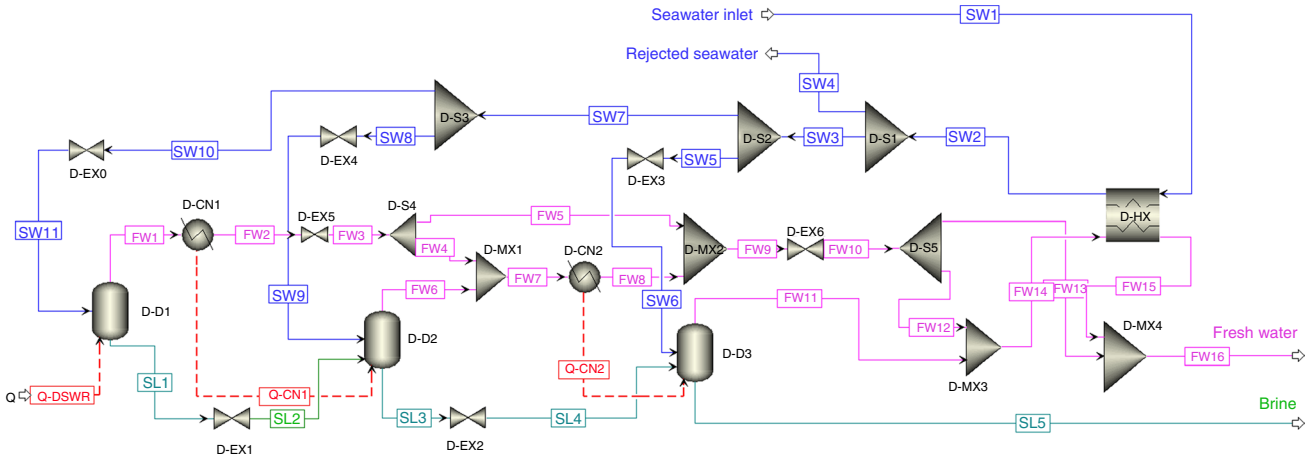

Fig. 5 Aspen Plus flowchart for the desalination unit (DSWR)

Table 9 Stream properties of SRC for the steam streams

# Units	$\dot{m}_j$ /kg s^{-1}	T_j /K	P_j /kPa	h_j /kJ kg^{-1}	s_j /kJ kg^{-1} K^{-1}	$ex_{ph,j}$ /kJ kg^{-1}	$ex_{ch,j}$ /kJ kg^{-1}	$ex_{t,j}$ /kJ kg^{-1}
A1	6	310.6	5	− 15,974.5	− 8.885	8.8	527.3	536.1
A2	6	310.6	500	− 15,973.8	− 8.885	9.4	527.3	536.7
A3	6	359.3	500	− 15,739.5	− 8.276	62.2	527.3	589.5
A4	6	410.0	500	− 15,491.0	− 7.717	143.9	527.3	671.3
A5	6	425.8	500	− 15,223.6	− 7.129	236.1	527.3	763.5
A6	6	510.1	7100	− 14,960.5	− 6.758	388.6	527.3	915.9
A7	6	810.0	7100	− 12,479.3	− 2.532	1610.0	527.3	2137.3
A8	6	611.1	1700	− 12,849.0	− 2.423	1207.5	527.3	1734.8
A9	6	800.0	1700	− 12,442.2	− 1.843	1441.5	527.3	1968.8
A10	4.374	310.6	5	− 13,523.2	− 1.379	222.1	527.3	749.4
A11	0.6	724.3	1000	− 12,597.6	− 1.805	1274.7	527.3	1802.1
A11-E	6	724.3	1000	− 12,597.6	− 1.805	1274.7	527.3	1802.1
A11-T	5.4	724.3	1000	− 12,597.6	− 1.805	1274.7	527.3	1802.1
A12	0.54	657.1	600	− 12,733.4	− 1.768	1128.0	527.3	1655.3
A12-E	5.4	657.1	600	− 12,733.4	− 1.768	1128.0	527.3	1655.3
A12-T	4.86	657.1	600	− 12,733.4	− 1.768	1128.0	527.3	1655.3
A13	0.486	574.5	300	− 12,897.3	− 1.717	948.9	527.3	1476.3
A13-E	4.86	574.5	300	− 12,897.3	− 1.717	948.9	527.3	1476.3
A13-T	4.374	574.5	300	− 12,897.3	− 1.717	948.9	527.3	1476.3
A14	0.6	453.1	1000	− 15,271.7	− 7.284	234.2	527.3	761.5
A15	0.6	432.6	600	− 15,271.7	− 7.251	224.3	527.3	751.6
A16	1.14	432.6	600	− 14,069.3	− 4.575	628.8	527.3	1156.1
A17	1.14	432.6	600	− 15,377.1	− 7.485	188.8	527.3	716.1
A18	1.14	408.1	300	− 15,377.1	− 7.446	177.2	527.3	704.5
A19	1.626	408.1	300	− 14,635.9	− 5.705	399.1	527.3	926.5
A20	1.626	408.1	300	− 15,500.6	− 7.737	140.2	527.3	667.5
A21	1.626	310.6	5	− 15,500.6	− 7.434	50.0	527.3	577.4
A22	6	310.6	5	− 14,059.1	− 3.020	175.5	527.3	702.8

Table 10 Stream properties for the GBC for the gas mixture, air, and fuels

#	$\dot{m}_j$	T_j	P_j	h_j	s_j	$ex_{ph,j}$	$ex_{ch,j}$	$ex_{t,j}$
Units	/kg s^{-1}	/K	/kPa	/kJ kg^{-1}	/kJ kg^{-1} K^{-1}	/kJ kg^{-1}	/kJ kg^{-1}	/kJ kg^{-1}
B1	0.50	293.2	105.0	− 5.3	0.122	3.1	4.5	7.6
B2	32.35	1273.2	200.0	− 2066.8	1.437	858.3	83.2	941.5
B3	32.35	948.2	200.0	− 2527.0	1.020	522.3	83.2	605.6
B4	32.35	892.7	200.0	− 2602.4	0.938	471.3	83.2	554.5
B5	32.35	489.2	200.0	− 3120.5	0.170	182.4	83.2	265.6
F1	0.20	293.2	200.0	− 3510.4	− 3.991	288.3	67,889.1	68,177.4
F2	1.00	293.2	2000.0	− 3514.5	− 7.283	1265.7	67,889.1	69,154.8
F3	0.25	293.2	800.0	− 3511.8	− 5.967	876.0	67,889.1	68,765.1
FW	60.00	343.2	200.0	− 15,817.6	− 8.468	41.4	527.3	568.7
G1	30.00	298.2	101.3	− 0.2	0.150	0.0	4.5	4.5
G2	30.00	475.3	429.5	180.3	0.208	163.0	4.5	167.5
G3	30.00	375.3	430.0	77.6	− 0.034	132.8	4.5	137.2
G4	30.00	594.6	1823.2	305.1	0.025	342.7	4.5	347.2
G5	6.00	594.6	1823.2	305.1	0.025	342.7	4.5	347.2
G6	24.00	594.6	1823.2	305.1	0.025	342.7	4.5	347.2
G7	31.65	1473.2	1823.0	− 1196.7	1.036	1267.7	275.1	1542.8
G8	31.65	1373.2	1823.0	− 1343.4	0.933	1151.7	275.1	1426.9
G9	31.65	1165.4	750.0	− 1642.0	0.979	839.4	275.1	1114.5
G10	31.65	1268.6	750.0	− 1495.4	1.099	950.1	275.1	1225.3
G11	31.65	1099.4	350.0	− 1734.6	1.138	699.2	275.1	974.4
G12	31.65	1003.9	200.0	− 1866.2	1.190	552.2	275.1	827.4
M1	0.65	286.3	101.3	− 11,232.8	− 6.771	− 4.7	26,276.8	26,272.0
M2	0.65	473.2	1823.0	− 5577.5	0.044	1175.8	28,565.8	29,741.6
M3	0.65	673.2	1823.0	− 5317.8	0.717	1501.5	28,220.8	29,722.3
M4	6.65	923.2	1823.0	− 2225.6	0.388	720.0	491.1	1211.1
S1	0.40	293.2	101.3	− 16,058.4	− 9.127	− 3.0	527.3	524.3
SW	60.00	285.2	200.0	− 16,096.9	− 9.243	− 7.0	527.3	520.3
W1	400.00	288.2	500.0	− 15,907.2	− 9.203	1.2	527.3	528.5
W2	400.00	295.0	500.0	− 15,878.5	-9.104	0.5	527.3	527.8

heated by D-HX to 47 ℃ at SW2. Some of 36 kg s^{-1} will be rejected to the sea, while the remaining will be fed to the stages with an equal amount of 8 kg s^{-1}, as shown in Table 11. The first stage D-D1 has a pressure of 22.7 kPa and a temperature of 65 ℃. The following two stages have a pressure of 16.3 kPa and 11.4 kPa for D-D2 and D-D3, respectively. The temperatures of the last two stages are 56.5 ℃ (FW6) and 50 ℃ (FW11). The brine exits the first stage D-D1 at 1.1 kg s^{-1} and 65 ℃ (SL1), the second stage D-D2 at 2.4 kg s^{-1} and 57.5 ℃ (SL3), and the third stage D-D3 at 3.7 kg s^{-1} and 50 ℃ with salinity being 0.229 kg kg^{-1}. The freshwater exits the desalination system at FW16 with a flow rate of 20.3 kg s^{-1}, 48.2 ℃ and 11.3 kPa with a salinity of 7.1E−25, which is negligible. The steam enters the first stage at S-IN of 7.4 kg s^{-1}, 110 ℃, and 100 kPa and leaves it at 99.6 ℃ to produce heat of 16,758 kW to the first stage.

The component performance for the SRC and GBC is displayed in Table 12 and for the DSWR in Table 13. For the SRC, the turbine power is 1996.8 kW for HP-ST1, 839.1 kW for IP-ST2, and 3840 kW for LP-ST3 combined. The required power of the first pump is 4.3 kW and 1578.6 for the second pump. All thermal efficiencies of turbomachinery components are assumed to be the same 85% isentropic and 90% mechanical efficiency. The required heat for the boiler heat exchanger (HXBL) and reheater (HXRH) is 14,887 kW and 2440.8 kW, respectively. The rejected heat by the condenser (CN) is 11492 kW. The feedwater heaters have a duty of 1604 kW for the CFH1, 1490 kW for the CFH2, and 1406 kW for CFH3. The desalination unit (DSWR) has a required heat of 16,758 kW. All the heat exchangers and condensers have 100% thermal efficiency because there are no heat loss and no pressure drop in the flow. The boiler burner (BRBL) is 7092 kW, with a thermal efficiency of about 59%. The sum of exergy destruction rates for turbines and pumps is 2245.3 kW, while for the heat exchangers and feedwater heaters it is 31596.7, and the maximum rate is recorded for HXBL to be 22,271.3 kW.

Table 11 Stream properties of desalination unit DSWR

# Units	$\dot{m}_j$ /kg s^{-1}	T_j /K	P_j /kPa	h_j /kJ kg^{-1}	s_j /kJ kg^{-1} K^{-1}	ex_j kJ kg^{-1}	q [−]	y_{H_2O} [−]	y_{NACL} [−]
FW1	6.9	338.0	22.7	− 13,349.0	− 1.54	275.4	1	1	0
FW2	6.9	335.8	22.7	− 15,708.0	− 8.56	9.1	0	1	0
FW3	6.9	328.6	16.3	− 15,708.0	− 8.56	8.8	0.013	1	0
FW4	2.8	328.6	16.3	− 15,708.0	− 8.56	8.8	0.013	1	0
FW5	4.1	328.6	16.3	− 15,708.0	− 8.56	8.8	0.013	1	0
FW6	6.7	330.5	16.2	− 13,362.8	− 1.43	227.9	1	1	0
FW7	9.5	328.6	16.2	− 14,043.9	− 3.50	164.2	0.715	1	0
FW8	9.5	328.6	16.3	− 15,738.1	− 8.65	6.0	0	1	0
FW9	13.6	328.6	16.3	− 15,729.0	− 8.62	6.9	0.004	1	0
FW10	13.6	321.3	11.4	− 15,729.0	− 8.62	6.3	0.017	1	0
FW11	6.7	323.0	11.3	− 13,376.7	− 1.31	177.3	1	1	0
FW12	9.5	321.3	11.4	− 15,729.0	− 8.62	6.3	0.017	1	0
FW13	4.1	321.3	11.4	− 15,729.0	− 8.62	6.3	0.017	1	0
FW14	16.2	321.2	11.3	− 14,756.1	− 5.60	77.0	0.424	1	0
FW15	16.2	321.2	11.3	− 15,279.6	− 7.22	39.0	0.205	1	0
FW16	20.3	321.2	11.3	− 15,369.9	− 7.51	32.4	0.167	1	0
S-IN	7.4	383.0	100.0	− 13,266.5	− 1.99	492.8	1	1	0
S-OUT	7.4	372.6	100.0	− 15,553.6	− 8.13	33.6	0	1	0
SL1	1.1	338.0	22.7	− 13,266.9	− 6.19	30.4	0	0.749	0.251
SL2	1.1	330.7	16.3	− 13,266.9	− 6.18	28.1	0.008	0.749	0.251
SL3	2.4	330.5	16.2	− 13,451.0	− 6.41	24.3	0	0.766	0.234
SL4	2.4	323.1	11.4	− 13,451.0	− 6.40	22.0	0.009	0.766	0.234
SL5	3.7	323.0	11.3	− 13,529.4	− 6.53	19.6	0	0.771	0.229
SW1	60.0	285.0	105.0	− 15,574.1	− 8.87	0.5	0	0.965	0.035
SW2	60.0	320.0	105.0	− 15,432.3	− 8.41	4.2	0	0.965	0.035
SW3	24.0	320.0	105.0	− 15,432.3	− 8.41	4.2	0	0.965	0.035
SW4	36.0	320.0	105.0	− 15,432.3	− 8.41	4.2	0	0.965	0.035
SW5	8.0	320.0	105.0	− 15,432.3	− 8.41	4.2	0	0.965	0.035
SW6	8.0	320.0	100.0	− 15,432.3	− 8.41	4.1	0	0.965	0.035
SW7	16.0	320.0	105.0	− 15,432.3	− 8.41	4.2	0	0.965	0.035
SW8	8.0	320.0	105.0	− 15,432.3	− 8.41	4.2	0	0.965	0.035
SW9	8.0	320.0	16.3	− 15,432.3	− 8.41	4.0	0	0.965	0.035
SW10	8.0	320.0	105.0	− 15,432.3	− 8.41	4.2	0	0.965	0.035
SW11	8.0	320.0	22.7	− 15,432.3	− 8.41	4.0	0	0.965	0.035

For the GBC, as shown in Table 12, the compressor power is 6017 kW for LP-C1 and 7584 kW for HP-C2, and the turbine power is 8506 kW, 6815.6 kW and 4163.2 kW for HP-T1, LP-T2, and P-T3, respectively. The rejected heat of the intercooler (IC) is 3079.5 kW, and the required heat of the combustion chamber (CC) is 26885.8 kW. The actual air-to-fuel ratio is 2.5 kg_a kg_f^{-1}, while the theoretical air-to-fuel ratio is 1.98 kg_a kg_f^{-1}. The required heat of SOFC is 13174.4 kW, and the rejected heat of SR and WGS is 3675.9 kW and 168.8 kW, respectively. The electric efficiency of SOFC is 90.04%, and its thermal and exergetic efficiencies are 29.4% and 43.5%. All the mixers, splitters, and expansion valves require no power nor heat with negligible exergy destruction rates. This hybrid combined engine's total exergy destruction rate is about 146,425 kW.

The DSWR components are also analyzed in Table 13. The input heat from the boiler to DSWR is 16758 kW, which is the required heat for D-D1 flash stage. The second and third flashes need an input heat of 16,238 kW and 16,061.9 kW for D-D2 and D-D3, respectively. The heat exchanger of D-HX has a duty of 8505.2 kW and a maximum destruction rate with a minimum exergetic efficiency of less than 40%. The total exergy destruction rate of DSWR is 1201.3 kW. The GOR is 2.89 since the steam mass flow rate is 7.35 kg s^{-1} entering at 110 ℃ and 100 kPa to release its heat to the DSWR and leaving it at the saturated liquid. Based on the datasheet of the Aframax ship, the freshwater

Table 12 Component performance for the SRC and GBC engines

C# Units	$\dot{Q}_k$ /kW	$\dot{W}_k$ /kW	$\dot{E}x_{D,k}$ /kW	$\eta_{th,k}(\eta_{e,k})$ [%]	ψ_k [%]
HP-C2	0.0	7584.0	1286.2	76.5	83.0
HP-ST1	0.0	1996.8	417.9	76.5	79.1
HP-T1	0.0	8506.0	1378.8	76.5	83.8
IP-ST2	0.0	839.1	161.6	76.5	80.8
LP-C1	0.0	6017.0	6017.0	76.5	81.3
LP-ST3	0.0	659.9	132.6	76.5	83.3
LP-ST4	0.0	716.7	153.5	76.5	82.4
LP-ST5	0.0	2464.2	714.9	76.5	77.5
LP-T2	0.0	6815.6	1124.8	76.5	85.8
P-T3	0.0	4163.2	490.1	76.5	89.5
P1	0.0	4.3	0.8	76.5	81.2
P2	0.0	1578.6	664.1	76.5	57.9
IC	3079.5	0.0	2056.9	100.0	66.7
CN	11,492.2	0.0	1465.8	100.0	68.7
CFH1	1604.5	0.0	1568.7	100.0	22.6
CFH2	1490.9	0.0	965.5	100.0	45.8
CFH3	1406.0	0.0	800.3	100.0	57.6
DSWR	16,758.3	0.0	1201.3	86.3	35.4
GTHX	4642.2	0.0	7372.4	100.0	86.0
HXBL	14,887.4	0.0	22,271.3	100.0	46.8
HXRH	2440.8	0.0	3323.7	100.0	84.4
BRBL	7092.0	0.0	14,798.8	58.7	67.3
CC	26,885.8	0.0	58,158.5	52.8	45.6
SOFC	13,174.4	3878.0	18,392.3	29.4 (90.04)	43.5
SR	3675.9	0.0	894.4	24.4	60.3
WGS	168.8	0.0	81.5	6.3	86.7
EX1	0.0	0.0	6.0	100.0	98.7
EX2	0.0	0.0	13.2	100.0	98.4
EX3	0.0	0.0	146.6	100.0	86.5
GTMX	0.0	0.0	324.2	100.0	98.1
MX1	0.0	0.0	26.9	100.0	98.0
MX2	0.0	0.0	14.2	100.0	99.1
MX3	0.0	0.0	0.0	100.0	100.0
GTSP	0.0	0.0	0.0	100.0	100.0
SP1	0.0	0.0	0.0	100.0	100.0
SP2	0.0	0.0	0.0	100.0	100.0
SP3	0.0	0.0	0.0	100.0	100.0

tanks are approximately 150 m^3, which means the freshwater is reaching its required capacity after 2.1 h to fill 153.7 m^3. Also, the ship demands 600 m^3 of technical freshwater tanks, which can be achieved after 8.5 h to fill 622 m^3. The thermal and exergetic efficiency of DSWR unit is 86.3% and 31.6%, respectively.

Table 13 Component units for desalination unit (DSWR)

C# Units	$\dot{Q}_k$ /kW	$\dot{E}x_{D,k}$ /kW	$\eta_{th,k}$ [%]	ψ_k [%]
D-CN1	16,238.0	222.7	100.0	89.8
D-CN2	16,061.9	4.9	100.0	99.7
D-HX	8505.2	366.3	100.0	37.4
D-D1	16,758.0	85.5	88.2	95.7
D-D2	16,238.0	69.3	76.9	95.7
D-D3	16,061.9	65.6	68.1	94.7
D-EX0	0.0	0.9	100.0	97.2
D-EX1	0.0	4.7	100.0	90.2
D-EX2	0.0	4.7	100.0	90.2
D-EX3	0.0	0.0	100.0	99.9
D-EX4	0.0	1.1	100.0	96.9
D-EX5	0.0	2.1	100.0	96.7
D-EX6	0.0	6.9	100.0	92.5
D-MX1	0.0	0.3	100.0	100.0
D-MX2	0.0	0.0	100.0	100.0
D-MX3	0.0	1.3	100.0	99.9
D-MX4	0.0	0.5	100.0	99.9
D-S1	0.0	0.0	100.0	100.0
D-S2	0.0	0.0	100.0	100.0
D-S3	0.0	0.0	100.0	100.0
D-S4	0.0	0.0	100.0	100.0
D-S5	0.0	0.0	100.0	100.0

Effect of fuel blends on engine subsystems

Five fuel blends are chosen, and hydrogen is the basis of this combination. The net power and net required heat are shown in Fig. 6. The net power of the SRC is constant at 5094 kW for all fuel blends since the working fluid is steam. The net power of the GBC is a maximum of 5884 kW using the MF1 and a minimum of 4933 kW using MF3 and MF4. However, the minimum power of the SOFC is given to be 3878 kW using MF1, and maximum power is 6667 kW using MF5, as shown in Fig. 6a. The required heat of the engine is by the BRBL, CC, and net heat of SOFC, including the reforming and water shifting processes, as shown in Fig. 6b. The BRBL heat is its highest value of 7486 kW using MF2 and minimum value of 2323 kW using MF5 for combustion at 200 kPa and 1273 K. However, this trend changes in the CC since the minimum heat is achieved by MF1 of 26,886 kW and maximum heat is fulfilled by MF5 of 36,533 kW. The net heat of SOFC is 9330 kW using MF1 increased to its maximum of 12,036 kW using MF5. Therefore, the total engine power is calculated from 14,856 kW of MF1 to 16,780 kW of MF5, while the total required heat is obtained to be a minimum of 43,308 kW by MF1 and a maximum of 53,507 kW by MF4.

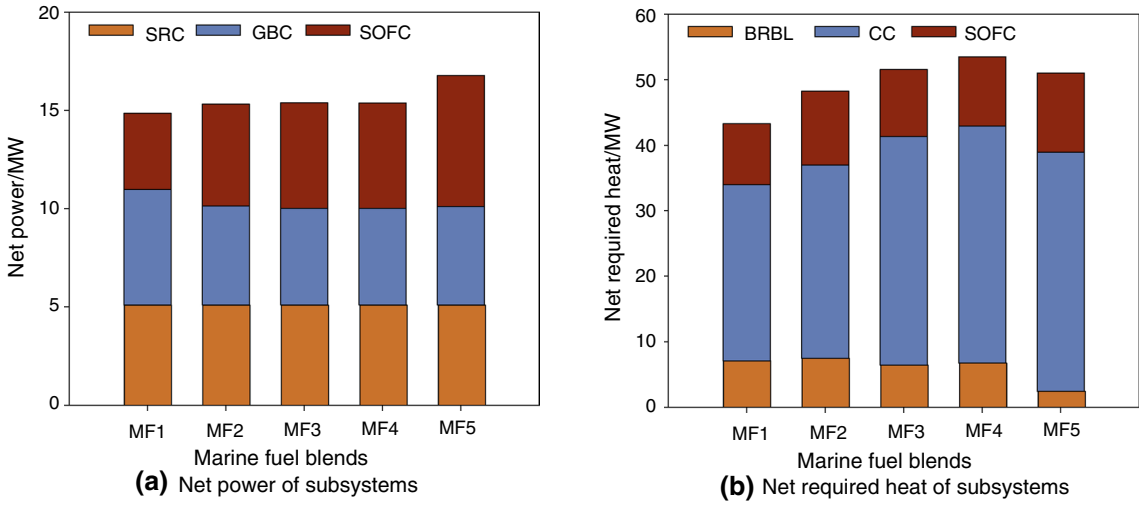

Fig. 6 Net power and net required heat for three marine subsystems

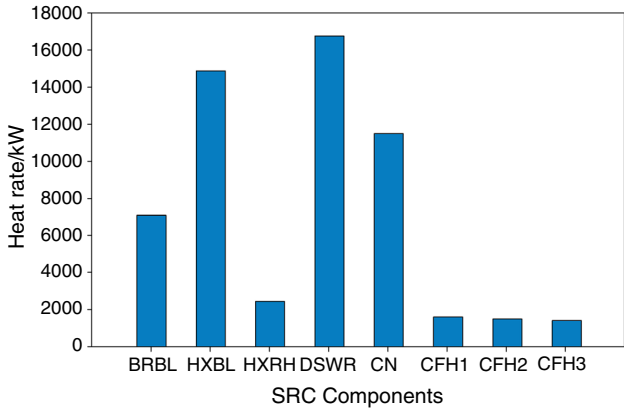

Fig. 7 Heat rates of SRC components for all fuels

The heat rates of SRC components are displayed in Fig. 7. The burner boiler added heat of 7092 kW using MF1 and varied with fuel blends, as discussed previously. However, the duty of heat exchangers of the boiler, reheater, condensers, feedwater heaters, and desalination remains constant despite the fuel change. The primary source of added heat to the SRC is HXBL of 14,887 kW and HXRH of 2440 kW. The feedwater heaters save this much heat (about 4501 kW) from the HXBL. The condenser rejects a heat of 11,492 kW from the steam to reach a saturated liquid, and the desalination uses heat of 16,758 kW from the waste energy of exhaust gases.

The overall performance of each subsystem is also estimated by considering the exergy destruction rates and

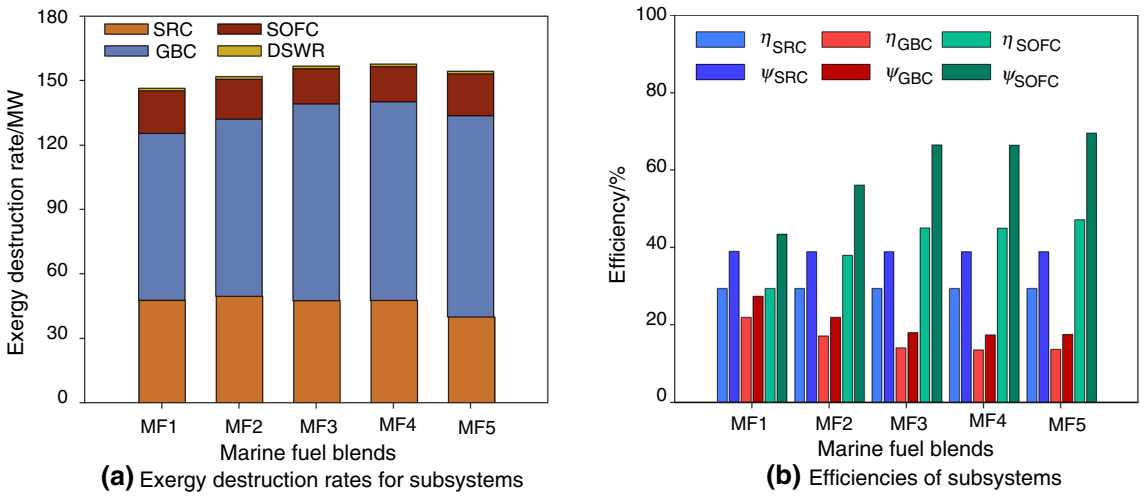

Fig. 8 Exergy destruction rates and thermal and exergetic efficiencies for three subsystems

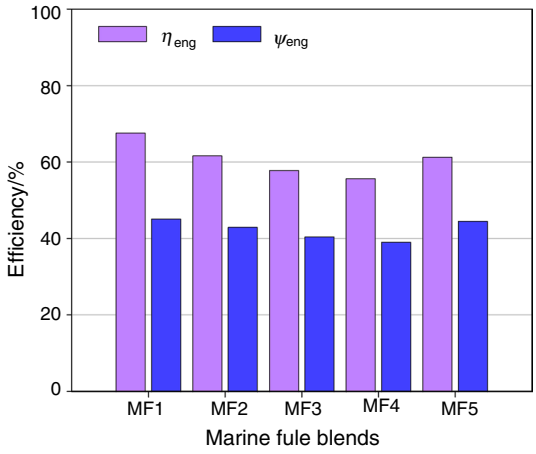

Fig. 9 Overall energetic and exergetic efficiency of the engine

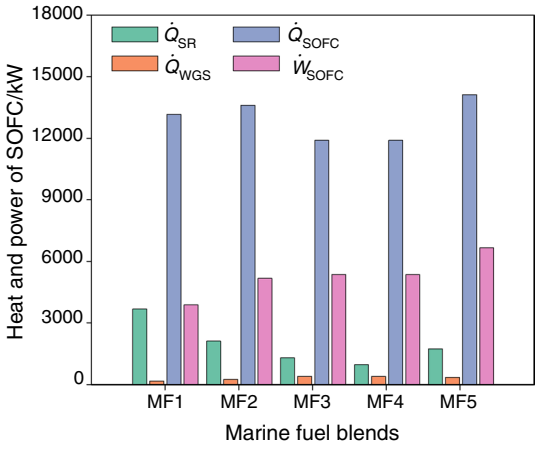

Fig. 10 Distribution of heat and power of SOFC

energetic and exergetic efficiencies, as shown in Fig. 8. The desalination DSWR has a constant destruction rate of 1201 kW. The GBC has a minimum destruction rate of 77,885 kW using MF1 and a maximum of 93,610 using MF5. On the contrary, the SRC has a minimum destruction rate of 39,990 kW using MF5 and a maximum of 494,948 kW using MF2. The SOFC has a maximum and a minimum exergy destruction rate of 19,692 kW and 16,496 kW of MF1 and MF3, respectively. The total destruction rate of the whole engine is more than 145 MW with a maximum of 157,737 kW using MF4, as shown in Fig. 8a. The constant net power and heat of SRC result in unchanging thermal efficiency of 29.4% and unchanging exergetic efficiency of 38.9%. In comparison, the GBC achieves higher thermal and exergetic efficiency of 21.9% and 27.4%, respectively, using MF1 because of its maximum power and minimum heat of CC and destruction rate. For the SOFC, the maximum performance is obtained by using MF5 to be 47.2% and 69.6%, respectively, as shown in Fig. 8b.

The overall thermal efficiency of the proposed engine is more than 55% and close to 70%, while the exergetic efficiency of the engine is an average of 43%, as shown in Fig. 9. The performance of this new engine is evaluated as the ratio of useful energy sources, such as net power and energy of freshwater to the required energy as heat of CC, net duty of SOFC, heat of BRBL, as shown in Fig. 5b. The hybrid combined marine engine has a maximum energetic efficiency of 67.7% using MF1 and the maximum exergetic efficiency of 45.3%. MF1, MF2, and MF5 positively impacted the engine performance by more than 60% thermal efficiency and more than 43% exergetic efficiency. However, the new engine has minimum performance using MF4 (dimethyl ether and hydrogen) for 56% thermal efficiency and 39% exergetic efficiency.

Effect of fuel blends on the fuel cell

The marine fuel blends significantly impact SOFC since the fuel cell counts on the Gibbs energy of reactants and products of the fuels and the amount of hydrogen produced in the reforming and water shifting reactors. The SR heat varies from a minimum of 968 kW of MF4 to a maximum of 3676 kW of MF2, while the minimum heat WGS is obtained by MF1 at 169 kW, and its maximum heat is given by 397 by MF3 and MF4, because they have a similar amount of water and produced carbon monoxide and produced hydrogen, as shown in Fig. 10. The heat of the electrochemical reaction of hydrogen and oxygen in the anode and cathode electrodes is produced within a range between 11,902 kW (MF3 and MF4) and 14,137 kW (MF5). This rejected massive heat will subtract the exothermic reactions of SR and WGS to produce the overall heat rejection of SOFC. The net power of SOFC varies from a minimum value of 3878 kW (MF1) to a maximum value of 6667 kW (MF5).

The reason for this power is given in Fig. 11a. The electrochemical reaction produces a small cell voltage of an average of 0.4 V, because of the high operating pressure of 1823 kPa. Also, MF1 makes the fuel cell generate a cell voltage of 0.30 V compared to 0.44 V of MF5. The loss voltage that comes from activation losses, ohmic losses, and concentration losses altogether is 0.03 V for all the fuel blends with a still change of ± 0.001. This represents the high electric efficiency of SOFC to be an average of 92.5%, as presented in Fig. 11a. The SOFC power can only be obtained using 34 stacks for MF1 and MF2, 31 stacks for MF3 and MF4, and 36 stacks for MF5, as shown in Fig. 11b. Also, the amount of required hydrogen in SOFC has an average of 72.3 mol s^{-1}, which is about 72% of resultant hydrogen from the inlet fuel blend of F3 and reforming and water gas shifting processes. The SOFC system was able to increase the power of GBC from an average of 5165–10,452 kW and

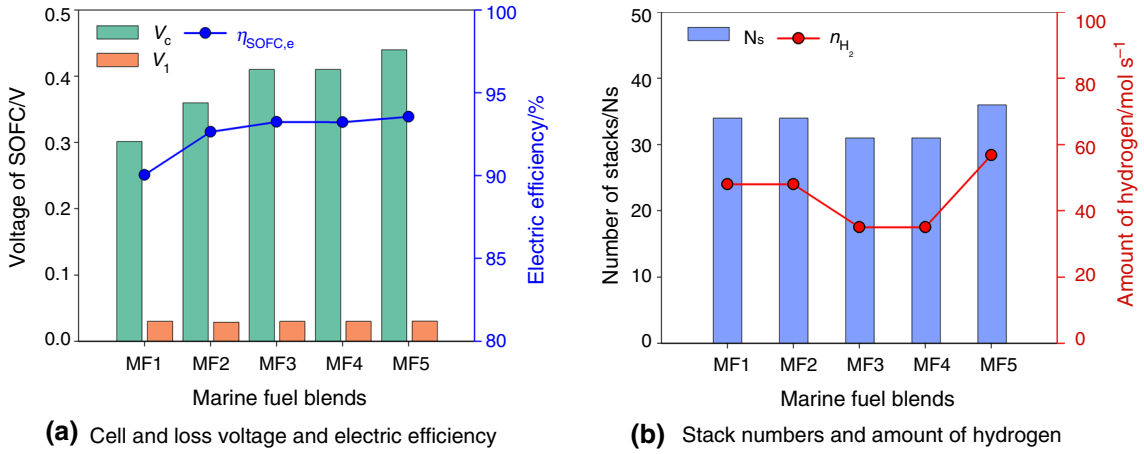

Fig. 11 Electric performance of SOFC and required stack numbers and amount of hydrogen in SOFC

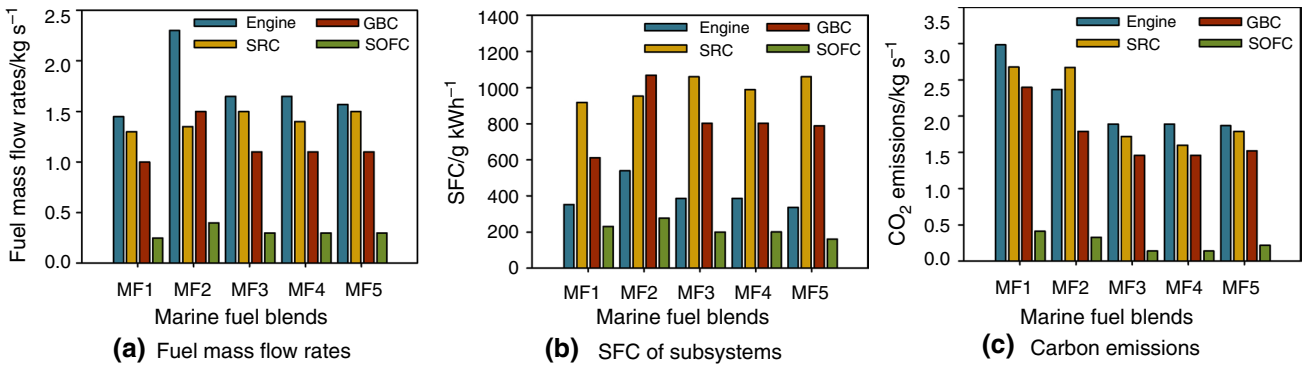

Fig. 12 Fuel mass flow rates, SFC, and carbon emissions of three marine subsystems

increase the efficiency from an average of 16% to 25%. The hybridization of GBC was performed by taking a small fraction of the intake air after the HP-C2 (a constant splitting ratio of 0.2) and a small amount of fuel about 25%, which is a great benefit of enhancing engine performance with less mechanical moving parts and less maintenance.

Fuel consumption and carbon emissions

Other parameters should be considered in analyzing the engine performance: fuel consumption and carbon emissions. The SRC burner uses the exhaust of GBC by G12 stream combusting with a fuel blend of F1 stream and air of B1 stream. However, in this analysis, the G12 is cancelled, and the SRC must count fully on the fuel blend of F1 and air of B1 only. Therefore, the air mass flow rate of B1 increases 30 kg s^{-1} to produce the same power of 5093.7 kW. Hence, each system was operating alone and compared with the hybrid combined engine using the same fuel, as shown in Fig. 12. The fuel mass flow rates of SRC vary from 1.3 to 1.5 kg s^{-1} with a minimum record for MF1. The GBC uses 1 kg s^{-1} for MF1 and 1.1 kg s^{-1} for MF3 to MF5 and 1.5 kg s^{-1} for MF2. The SOFC consumes 0.4 kg s^{-1} and less with a minimum of MF1 (0.25 kg s^{-1}) and a maximum of MF2 (0.4 kg s^{-1}). The total fuel flow rate for the proposed engine reaches its maximum value of 2.30 kg s^{-1} using MF2 and a minimum value of 1.45 kg s^{-1} using MF1, while the remaining MF3 to MF5 has an average of 1.62 kg s^{-1}, as shown in Fig. 12a. The specific fuel consumption (SFC) is estimated for the individual subsystem and overall engine as shown in Fig. 12b. The average of SFC is 996.5 g kWh^{-1} for the SRC, 815 g kWh^{-1} for the GBC, and 215.1 g kWh^{-1} for the SOFC, while the average of SFC for the whole engine is 400 g kWh^{-1} with a minimum of 337 g kWh^{-1} by the MF5 and a maximum value of 540 g kWh^{-1} by MF2. The designed engine's carbon emissions are slightly higher, with an average of 2.2 kg s^{-1} compared to 2.1 kg s^{-1} for SRC, 1.7 kg s^{-1} for the GBC, and 0.2 kg s^{-1} for the SOFC. However, high emissions can be produced by fuel MF1 and MF2, as shown in Fig. 12c.

As previously mentioned, the Aframax ship demands a total power of 10,400 kW. If the SRC is operated only

Table 14 Comparison of traditional marine engines and sustainable fuels hybrid marine engines

Fuels	$\dot{W}_o$ /kW	$\dot{m}_f$ \kg s^{-1}	SFC_t /g kWh^{-1}	$CO_{2,t}$ /kg s^{-1}	η_t [%]	ψ_t [%]	Mass /kg
MGO	11,141.8	1.26	405.5	3.98	29.1	38.6	91,540
MF1	14,855.5 (↑33.3)	1.45 (↑15.5)	351.4 (↓13.4)	2.98 (↓25.0)	67.7 (↑133)	44.7 (↑15.8)	58,016 (↓36.6)
MF2	15,322.3 (↑37.5)	2.30 (↑83.3)	540.4 (↑33.3)	2.37 (↓40.5)	61.7 (↑112)	42.5 (↑10.1)	58,016 (↓36.6)
MF3	15,389.3 (↑38.1)	1.65 (↑31.5)	386.0 (↓4.8)	1.89 (↓52.5)	57.9 (↑98.9)	41.2 (↑6.9)	57,824 (↓36.8)
MF4	16,382.8 (↑38.1)	1.65 (↑31.5)	386.1 (↓4.8)	1.89 (↓52.3)	55.8 (↑91.7)	39.9 (↑3.5)	57,824 (↓36.8)
MF5	16,779.7 (↑50.6)	1.57 (↑25.1)	336.8 (↓16.9)	1.87 (↓53.0)	61.4 (↑111)	46.1 (↑19.5)	58,144 (↓36.5)

using the MGO-DMA, the steam mass flow rate will be 13.5 kg s^{-1}, the fuel mass flow rate will be 1.26 kg s^{-1}, and the air mass flow rate will be 18.5 kg s^{-1}. This operation will generate a net power of 11,141.8 kW and a thermal and exergetic efficiency of 29.1% and 38.6%, respectively, as shown in Table 14. Also, the carbon emissions will be 3.98 kg s^{-1}, which doubles the emissions of the proposed system. On the contrary, this new marine engine emits less carbon dioxide by 25% using MF1 and up to 53% using MF5. In addition, the SFC of this SRC operated by the MGO-DMA will be about 405.5 g kWh^{-1}. The proposed hybrid combined engine has increased the total power by between 30 and 50%, with an increase in fuel mass by 25%, except for MF2, which is increased by 83%. The SFC is decreased between 5 and 17% for all fuel blends except for MF2. Fortunately, carbon emissions have reduced significantly to about an average of 50%. In addition, the thermal performance has increased to more than double the traditional system with an increase in exergetic performance of 11%, as shown in Table 14.

The Aframax ship (WSD42 11 K) is operated using a diesel engine of Wärtsilä 6X62, which delivers an output power of 10,400 kW with a mass of 377,000 kg [25]. Suppose the existing engine is replaced by only a steam Rankine cycle engine. In that case, there are two major components that weigh significantly compared to others: a boiler model of Aalborg D for a capacity of 38,800 kW of steam weighs 55,000 kg [38] and a steam turbine model of MST050 for 5-30 MW weighs 36,540 kg [39]. Therefore, the total mass of SRC is 91540 kg, as shown in Table 14 in the first row. Nevertheless, the proposed engine uses the half capacity of the SRC only and is combined with SOFC units and GBC. Therefore, the SRC that delivers a total turbine power of 5094 kW can be operated by MST020 with a capacity of 1–5 MW weighing 15,420 kg and uses a required heat of 17,328 kW run by Aalborg D with a capacity of 17,600 kW weighing 25,000 kg. Hence, the total mass of SRC is 40420 kg, which is almost half the mass of only an SRC engine. The GBC can be operated by Taurus 60, which delivers 5740 kW weighing 15,420 kg [33]. Also, a one SOFC stack of 100 cells weighs 64 kg [36], so the total weight of 34 stacks is 2176 kg for MF1 and MF2. Therefore, the total mass of the proposed engine is 58016 kg for MF1 and MF2, and so on. This proposed engine weighed less than the traditional SRC only by 36% and less than the traditional diesel engine of 377,000 kg by 85%. In conclusion, the proposed engine is more efficient, has less environmental impact, less mass, and is more reliable.

Parametric studies

The parametric studies are performed on the SRC and GBC. The mass fraction of bleeding and the inlet air to GBC is considered. Changing the bleeding splitting ratio from 0.01 to 0.3 individually has decreased the net power of SRC from 6970 to 11,030 kW and required heat of the HXBL and HXRH from 20,110 to 11,030 kW, as shown in Fig. 13a and b. The splitting ratio of the first splitter (SP1) decreases the required heat and net power more than that of the second one and the third one. The thermal efficiency of SRC varies from 35 to 6% for SP1, 9% for SP2, and 12% for SP3, as shown in Fig. 13c.

The three splitters should receive the same amount from the turbine, not one more than another, to ensure an increase in SRC performance. The bleeding ratio of the three splitters varies simultaneously from 0.01 to 0.2, as shown in Fig. 14. The net power decreases from 7626 to 153 kW at the ratio of 0.185; after that, there is no produced power. However, the required heat declined from 22,840 to 7450 kW. The thermal efficiency slightly increases from 33.4 to 35% at a splitting ratio of 0.08 then drops to 1.5% at a splitting ratio of 0.185. That means increasing the splitting ratio decreases the required heat and net power, yielding in decreasing the cycle efficiency.

Another parameter preferred for this study is the intake air mass flow rate G1, as shown in Fig. 15. The variation in G1 mass flow rate from 20 to 40 kg s^{-1} raises the net power of GBC from 4780 to 6640 kW, but it spikes up the net required heat of the CC and IC from 23,280 to 27,340 kW and drops gradually to 7290 kW. This significant decrease in required heat exponentially increases the thermal efficiency of the GBC from 20 to 90%, theoretically, as shown in Fig. 15a. However, practically, more excess air than 50% in the combustion chamber can shut off the operation and delay the ignition of fuel. This variation can affect the hybrid

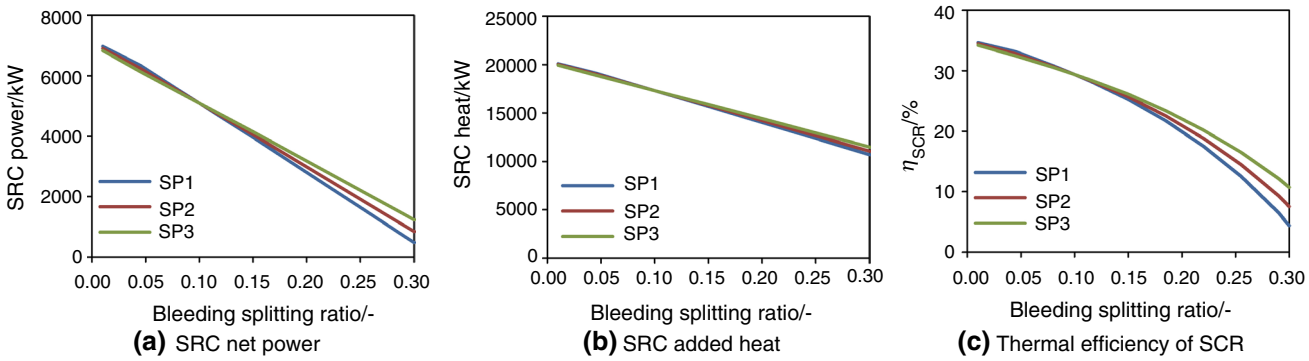

Fig. 13 Effect of individual bleeding ratio on net power, added heat, and thermal efficiency of SRC

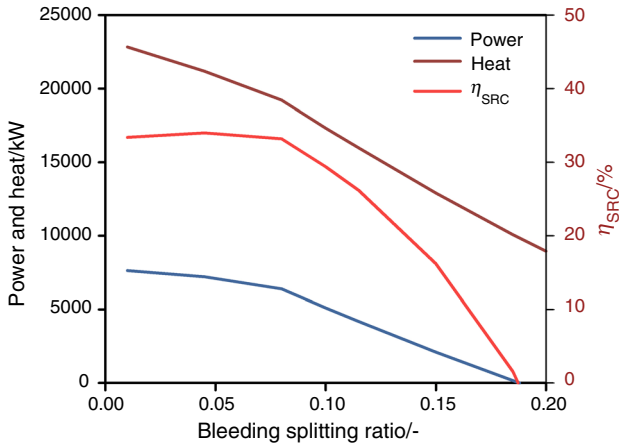

Fig. 14 Effect of bleeding ratio altogether on SRC performance

and combined engine by slightly increasing the total power from 13,750 to 15,620 kW. However, the total required heat of the BRBL and CC, and SOFC can gradually increase from 26,140 to 40,060 kW at 28 kg s^{-1} and then decrease to 23,660 kW, as shown in Fig. 15b. This heat trend is reversed in the overall thermal efficiency of the engine. The engine thermal efficiency changes from 53% to its lowest value of 36% and then rises to 66%.

Conclusions

This study presented and investigated a new design of a marine engine comprising of a steam Rankine cycle, gas Brayton cycle, and fuel cell systems. The engine is analyzed thermodynamically using Aspen Plus to assess its energy performance by utilizing five sustainable fuel blends. The following conclusions can be drawn from the study:

- The SRC can deliver a power of 5094 kW with a thermal efficiency of 29.4% and exergetic efficiency of 39%.
- The GBC can generate an average net power of 5165 kW with average thermal and exergetic efficiencies of 16% and 20.5%, respectively.

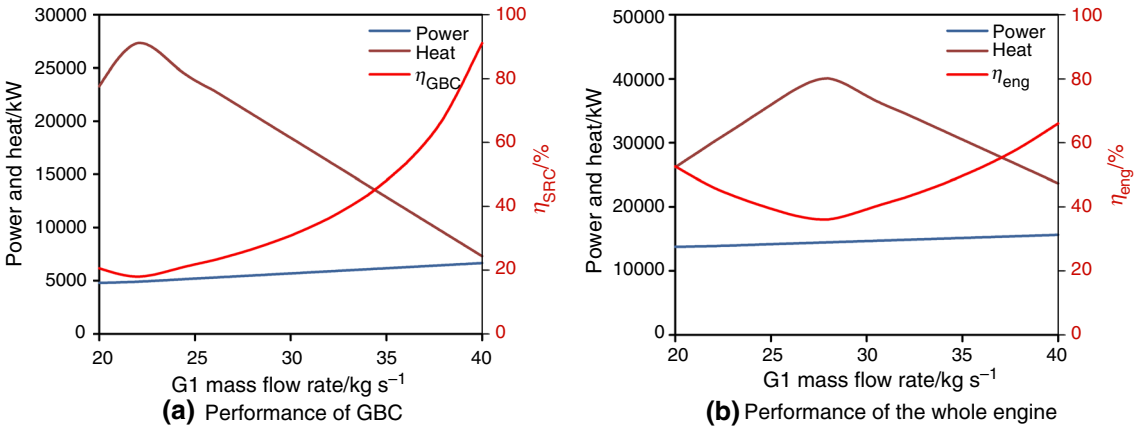

Fig. 15 Effect of G1 mass flow rates on the performance of GBC and the whole engine

- The SOFC can produce 5288 kW with average thermal, electric, and exergetic efficiencies of 41%, 60%, and 93%, respectively.
- The hybrid combined engine can generate a total power of 15,546 kW with average thermal and exergetic efficiencies of 61% and 43%, respectively.
- The maximum power is achieved using a mixture of methane, methanol, ethanol, dimethyl ether, and hydrogen (known as MF5), which can produce 16,780 kW electric power.
- A desalination unit uses the waste energy to produce 154 m^3 of freshwater within 2 h from the seawater with a thermal efficiency of 86%, exergetic efficiency of 32%, and a GOR of 2.9.
- The specific fuel consumption is decreased from 405 g kWh^{-1} using MGO-DMA to 337 g kWh^{-1} using MF5, which is a 16.8% improvement in fuel economy.
- Using sustainable fuels reduces carbon emissions by 53% and boosts thermal performance by about 110% and exergetic performance by around 11%, respectively.

This research promotes sustainable and green marine transportation because of the utilization of eco-friendly fuels and new powering systems, which enhances engine performance. However, this research focuses on thermodynamic analysis of the system under certain operating conditions, which might not be optimal. Some recommendations for future studies include conducting exergoeconomic analysis and exergoenvironmental analysis, multi-objective optimization of fuel substituents, and optimal system design to provide a comprehensive analysis of the new system.

Acknowledgements The authors acknowledge the financial support provided by Transport Canada through its Clean Transportation Program—Research and Development and the Natural Sciences and Engineering Research Council of Canada (NSERC).

Author contribution The corresponding author of paper entitled "Investigation of A Hybridized Combined Cycle Engine with SOFC System for Marine Applications" informs all the authors' individual contributions using the relevant Credit roles, which are listed below. Shaimaa Seyam "the corresponding author": methodology, software, date curation, writing original draft preparation, investigation, visualization, editingIbrahim Dincer: Supervision, conceptualization, funding acquisition, writing- Reviewing, and editingMartin Agelin-Chaab: co-supervision, conceptualization, and funding acquisition, writing-Reviewing, and editing.

References

1. Shi Y. Are greenhouse gas emissions from international shipping a type of marine pollution? Mar Pollut Bull. 2016;113:187–92. https://doi.org/10.1016/j.marpolbul.2016.09.014.
2. Khondaker AN, Rahman SM, Khan RA, Malik K, Muhyedeen MAR. Management of greenhouse gas emissions from maritime operations—challenges and mitigation opportunities. Int J Glob Warm. 2016;9:306–36. https://doi.org/10.1504/IJGW.2016.075447.
3. Jeong S, Woo JH, Oh D. Simulation of greenhouse gas emissions of small ships considering operating conditions for environmental performance evaluation. Int J Naval Architect Ocean Eng. 2020;12:636–43. https://doi.org/10.1016/j.ijnaoe.2020.07.006.
4. Chen J, Fei Y, Wan Z. The relationship between the development of global maritime fleets and GHG emission from shipping. J Environ Manage. 2019;242:31–9. https://doi.org/10.1016/j.jenvman.2019.03.136.
5. Ünlügençoğlu K, Kökkülünk G, Alarçin F. Estimation of shipping emissions via novel developed data collecting and calculation software: a case study for the Region of Ambarli Port. Int J Glob Warm. 2019;19:293–307. https://doi.org/10.1504/IJGW.2019.103723.
6. Muše A, Jurić Z, Račić N, Radica G. Modelling, performance improvement and emission reduction of large two-stroke diesel engine using multi-zone combustion model. J Therm Anal Calorim. 2020;141:337–50. https://doi.org/10.1007/s10973-020-09321-7.
7. Kanberoğlu B, Kökkülünk G. Assessment of CO_2 emissions for a bulk carrier fleet. J Clean Prod. 2021;283:124590. https://doi.org/10.1016/j.jclepro.2020.124590.
8. Vedachalam S, Baquerizo N, Dalai AK. Review on impacts of low sulfur regulations on marine fuels and compliance options. Fuel. 2022;310:122243. https://doi.org/10.1016/j.fuel.2021.122243.
9. Ampah JD, Yusuf AA, Afrane S, Jin C, Liu H. Reviewing two decades of cleaner alternative marine fuels: towards IMO's decarbonization of the maritime transport sector. J Clean Prod. 2021;320:128871. https://doi.org/10.1016/j.jclepro.2021.128871.
10. Moorthi M, Murugesan A, Alagumalai A. Effect of nanoparticles on DI-CI engine characteristics fueled with biodiesel–diesel blends—a critical review. J Therm Anal Calorim. 2022;147:9163–79. https://doi.org/10.1007/s10973-022-11234-6.
11. Hountalas DT, Mavropoulos GC, Katsanos C, Daniolos S, Dolaptzis I, Mastorakis N. Potential for efficiency improvement of four-stroke marine diesel gensets by utilisation of exhaust gas energy. Int J Glob Warm. 2016;10:133–57. https://doi.org/10.1504/IJGW.2016.077910.
12. Aghdoudchaboki Y, Khoshgard A, Salehi GR, Fazelpour F. Thermoeconomic assessment of a waste heat recovery system driven by a marine diesel engine for power and freshwater production. Int J Exergy. 2020;33:231–53. https://doi.org/10.1504/IJEX.2020.110841.
13. Jafarzad A, Asgari N, Ranjbar F, Mohammadkhani F. Thermodynamic assessment and optimization of the influences of the steam-assisted turbocharging and organic Rankine cycle on the overall performance of a diesel engine-based cogeneration integrated with a reverse osmosis desalination unit. Sustain Energy Technol Assess. 2021;46:101175. https://doi.org/10.1016/j.seta.2021.101175.
14. Pallis P, Varvagiannis E, Braimakis K, Roumpedakis T, Leontaritis AD, Karellas S. Development, experimental testing and techno-economic assessment of a fully automated marine organic Rankine cycle prototype for jacket cooling water heat recovery. Energy. 2021;228:120596. https://doi.org/10.1016/j.energy.2021.120596.
15. Ahn J, Lee S, Jeong J, Choi Y. Comparative feasibility study of combined cycles for marine power system in a large container ship considering energy efficiency design index (EEDI). Int J Hydrog Energy. 2021;46:31816–27. https://doi.org/10.1016/j.ijhydene.2021.07.068.
16. Tsougranis EL, Wu D. A feasibility study of organic Rankine cycle (ORC) power generation using thermal and cryogenic waste

energy on board an LNG passenger vessel. Int J Energy Res. 2018;42:3121–42. https://doi.org/10.1002/er.4047.
17. Gonca G. Thermo-ecological performance analysis of a double-reheat Rankine cycle steam turbine system (RCSTS) with open and close feed water heaters. Int J Exergy. 2018;25:117–31. https://doi.org/10.1504/IJEX.2018.089550.
18. Gude VG. Thermal desalination of ballast water using onboard waste heat in marine industry. Int J Energy Res. 2019;43:6026–37. https://doi.org/10.1002/ER.4647.
19. Singh OK. Combustion simulation and emission control in natural gas fuelled combustor of gas turbine. J Therm Anal Calorim. 2016;125:949–57. https://doi.org/10.1007/s10973-016-5472-0.
20. Long Y, Li G, Zhang Z, Wei W, Liang J. Hydrogen-rich gas generation via the exhaust gas-fuel reformer for the marine LNG engine. Int J Hydrog Energy. 2022;47:14674–86. https://doi.org/10.1016/j.ijhydene.2022.02.188.
21. Lion S, Taccani R, Vlaskos I, Scrocco P, Vouvakos X, Kaiktsis L. Thermodynamic analysis of waste heat recovery using Organic Rankine Cycle (ORC) for a two-stroke low speed marine diesel engine in IMO Tier II and Tier III operation. Energy. 2019;183:48–60. https://doi.org/10.1016/j.energy.2019.06.123.
22. Chitgar N, Emadi MA, Chitsaz A, Rosen MA. Investigation of a novel multigeneration system driven by a SOFC for electricity and fresh water production. Energy Convers Manag. 2019;196:296–310. https://doi.org/10.1016/j.enconman.2019.06.006.
23. Solar Turbines. Taurus 60 gas turbine generator set. Solar Turbines Incorporated 2018:DS60PG/0320/EO.
24. WARTSILA. Aframax tanker for oil and products: WSD42 111K 2014.
25. WARTSILA. WARTSILA Engines: WARTSILA X62 2014:1–2 datasheet.
26. Canada CE, Science E, Division T. Marine Diesel Fuel Oil 1999.
27. Guent MBV. Everything you need to know about marine fuels. Chevron Product Eng Dep. 2012;27:2009.
28. McCarty RD, Hord J, Roder HM. Selected properties of hydrogen (engineering design data). U.S. Department of Commerce/National Bureau of Standards; 1981.
29. Verhelst S, Turner JW, Sileghem L, Vancoillie J. Methanol as a fuel for internal combustion engines. Prog Energy Combust Sci. 2019;70:43–88. https://doi.org/10.1016/j.pecs.2018.10.001.
30. Pereira LG, Cavalett O, Bonomi A, Zhang Y, Warner E, Chum HL. Comparison of biofuel life-cycle GHG emissions assessment tools: The case studies of ethanol produced from sugarcane, corn, and wheat. Renew Sustain Energy Rev. 2019;110:1–12. https://doi.org/10.1016/j.rser.2019.04.043.
31. Li Q, Wu G, Johnston CM, Zelenay P. Direct dimethyl ether fuel cell with much improved performance. Electrocatalysis. 2014;5:310–7. https://doi.org/10.1007/s12678-014-0196-z.
32. Çengel YA, Boles MA. Thermodynamics: a engineering approach, 8th ed. USA: McGraw-Hill Education; 2015. https://doi.org/10.1109/MILCOM.2005.1605829.
33. Solar Turbines. Industry Leader for Gas Turbine Power 2022.
34. Midilli A, Akbulut U, Dincer I. A parametric study on exergetic performance of a YSZ electrolyte supported SOFC stack. Int J Exergy. 2017;24:173–200. https://doi.org/10.1504/IJEX.2017.087653.
35. Seyam S, Dincer I, Agelin-Chaab M. Development and assessment of a unique hybridized gas turbine locomotive engine operated by sustainable fuel blends. Fuel. 2022;330:125638. https://doi.org/10.1016/j.fuel.2022.125638.
36. O'Hayre R, Cha S-W, Colella WG, Prinz FB. Fuel cell fundamentals, 3rd ed. Hoboken, New Jersey: John Wiley & Sons Inc.; 2016.
37. Seyam S, Dincer I, Agelin-Chaab M. Development and assessment of a cleaner locomotive powering system with alternative fuels. Fuel. 2021;296:120529. https://doi.org/10.1016/j.fuel.2021.120529.
38. Alfa Laval. Aalborg D. Scarborough, Canada: 2015.
39. MAN Energy Solutions. Steam turbines. Augsburg, Germany: 2020. https://doi.org/10.1038/scientificamerican08131910-101supp.